Citation: Progressive environmental deterioration in NW Pangea leading to the Latest Permian Extinction, S.E. Grasby et al., 2015, Geological Society of America Bulletin, doi: dx.doi.org/10.1130/B31197.1.

Progressive environmental deterioration in NW Pangea leading to the Latest Permian Extinction

Stephen E. Grasby[1,2*], Benoit Beauchamp[2], David P.G. Bond[3], Paul Wignall[4], Cristina Talavera[5], Jennifer M. Galloway[1], Karsten Piepjohn[6], Lutz Reinhardt[6], Dierk Blomeier[7]

[1]Geological Survey of Canada, Natural Resources Canada 3303 33rd Street NW, Calgary, AB, T2L 2A7, Canada,

[2]Department of Geoscience, University of Calgary, 2500 University DR. NW, Calgary, AB, T2N 1N4, Canada

[3]Department of Geography, Environment and Earth Sciences, University of Hull, Hull HU6 7RX, United Kingdom

[4]School of Earth Sciences, University of Leeds, Woodhouse Lane, Leeds LS2 9JT, United Kingdom

[5]Department of Imaging and Applied Physics, Curtin University, Kent Street, Bentley, 6102, WA, Australia

[6]Bundesanstalt für Geowissenschaftern und Rohstoffe, Geozentrum Hannover, Stilleweg 2, D-30655 Hannover, Germany

[7]*Millennia Stratigraphic Consultants, 35 Swansfield Lechlade, Glos. GL7 3SF, United Kingdom*

*E-mail: sgrasby@nrcan.gc.ca

ABSTRACT

Stratigraphic records from northwestern Pangea provide unique insight into global processes that occurred during the Latest Permian Extinction (LPE). We examined a detailed geochemical record of the Festningen Section, Spitsbergen. A stepwise extinction is noted: 1) loss of carbonate shelly macrofauna, 2) loss of siliceous sponges in conjunction with an abrupt change in ichnofabrics as well as dramatic change in the terrestrial environment, and 3) final loss of all trace fossils. We interpret loss of carbonate producers as related to shoaling of the lysocline in relationship to building atmospheric CO_2 in higher latitudes. The loss of siliceous sponges is coincident the global LPE event and is related to onset of high loading rates of toxic metals (Hg, As, Co) that we suggest are derived from Siberian Trap eruptions. The final extinction stage is coincident with redox sensitive trace metal and other proxy data which suggest onset of anoxia, after the other extinction events. These results show a remarkable record of progressive environmental deterioration in NW Pangea during the extinction crises.

1.0 INTRODUCTION

The Latest Permian Extinction (LPE) represents a period of dramatic climate change associated with disruption of global biogeochemical cycles and the worst mass extinction event in Earth history. Over 90% of marine species and 70% of terrestrial vertebrates went extinct at this time (Erwin, 2006). While numerous extinction mechanisms have been proposed, growing evidence supports environmental effects associated with massive eruption of the Siberian Traps (Campbell et al., 1992; Grasby et al., 2011; Renne et al., 1995; Saunders and Reichow, 2009; Shen et al., 2011; Wignall, 2001). The original volume of the Siberian Traps and West Siberian rift system is difficult to estimate, but upper-end figures of 3 - 4 x 10^6 km^3 (Courtillot et al., 1999; Fedorenko et al., 2000) make this mega-scale eruption one of the largest in earth history.

Magma intruded through the Tunguska Basin, and was associated with combustion of organic rich sediments (Grasby et al., 2011; Reichow et al., 2009; Retallack and Jahren, 2008; Retallack and Krull, 2006; Svensen et al., 2009), along with release of large volumes of CO_2 (White and Saunders, 2005; Wignall, 2001), deleterious atmospheric gases (Beerling et al., 2007; Black et al., 2012; Black et al., 2014; Kaiho and Koga, 2013; Svensen et al., 2009), and toxic elements (Grasby et al., 2013a; Grasby et al., 2011; Sanei et al., 2012). Oxygen isotope records suggest that rapid global warming and extremely high ocean temperatures developed at this time (Romano et al., 2013; Sun et al., 2012), invoking a hothouse scenario (Kidder and Worsley, 2010; Retallack, 1999; Song et al., 2014). Acid ocean conditions may also have developed at this time (Beauchamp and Grasby, 2012; Heydari and Hassanzadeh, 2003; Kidder and Worsley, 2004, 2010; Liang, 2002; Payne et al., 2007). Global anoxia has long been suggested to be an important environmental stress associated with the LPE (Isozaki, 1997; Knoll et al., 1996; Wignall and Hallam, 1992; Wignall and Twitchett, 1996). While some regions show evidence of photic zone euxinia in the Tethys and Panthalassa (Grice et al., 2005; Hays et al., 2007; Kump et al., 2005; Xie et al., 2007), the extinction event has also been suggested to occur under at least locally oxic conditions in NW Pangea (Algeo et al., 2010; Knies et al., 2013; Proemse et al., 2013) and in Neotethys (Korte et al., 2004; Loope et al., 2013; Richoz et al., 2010) (Fig. 1a).

Given the above, the relative timing of various environmental stresses becomes critical to understanding the role they played during the mass extinction. To address this question we examined the Festningen section in Spitsbergen (Wignall et al., 1998), a shelf sea location on northern Pangean margin during Late Permian time (Figs. 1b,c). The Festningen section was one of the earliest locations where development of anoxia in association with the mass extinction event was demonstrated (Wignall et al., 1998). However, this study was based on a low sample density for carbon isotope data that did not provide clarity as to detailed biogeochemical events occurring during the extinction period. Subsequent work at other sites in Spitsbergen has pointed to the gradual development of anoxia across the LPE event (Dustira et al., 2013), as well as in correlative strata in the Sverdrup Basin (Grasby and Beauchamp, 2009). To elucidate the relative timing of various environmental stressors we have undertaken detailed analyses of the Festningen based on high resolution sampling through the LPE.

2.0 STUDY AREA

The Festningen section is located at Kapp Starostin, west of the mouth of Grønfjorden where it enters Isfjorden on Nordenskiöld Land, Spitsbergen (Fig. 1b). In Permian time the area formed part of a broad epicontinental shelf on the northwestern margin of Pangea (Fig. 1c), along with correlative strata from the Wandel Sea (North Greenland), the Sverdrup Basin (Canadian High Arctic), and the Barents Sea and Timan-Pechora Basin (Russia) (Stemmerik and Worsley, 2005). Spitsbergen was at a paleolatitude of ~40-45° N during the Middle to Late Permian (Golonka and Ford, 2000; Scotese, 2004).

2.1 Festningen Section

The Festningen section occurs as ~45° eastward dipping beds (Fig. 2) forming a ~7 km coastal section exposed in a low sea-cliff, including near continuous exposure of Carboniferous to Cenozoic strata, from Kapp Starostin to Festningsdodden. The section is located in the eastern part of the West Spitsbergen Fold and Thrust Belt, an intra-continental fold and thrust belt ranging over more than 300 km along the west coast from the Brøgger Peninsula in the North to the Sørkapp in the very South (CASE-Team, 2001; Dallmann et al., 1993; Maher and Craddock, 1988). The intense crustal shortening is a result of the northward directed movement of

Greenland against the Barents shelf during the Eocene, before Spitsbergen was finally separated from Greenland. The Festningen section is part of the steeply inclined short-limb of a kilometer-scale east-vergent fold structure. A sill cuts through the series (dating from the Cretaceous 124.7 Ma) (Corfu et al., 2013). Festningen was located in the central Spitsbergen region were Upper Permian sediments, deposited in a distal shelf setting, are thickest (Wignall et al., 1998) (Blomeier et al., 2013). Festningen represents the type-section for both the Kapp Starostin and Vardebukta formations which are examined here.

The Kapp Starostin Formation is a Middle to Late Permian unit that was deposited at a time of tectonic quiescence and passive subsidence following a major relative sea level drop coinciding with the Lower/Middle Permian boundary (Blomeier et al., 2013). An initial Roadian transgression led to the deposition of a widespread heterozoan carbonate (Vøringen Member), which was followed by a series of regressions and transgressions that led to the progradation of heterozoan carbonates and cherts over much of the Barents Shelf and Svalbard (Blomeier et al., 2013), as well as in the paleogeographically adjoining Sverdrup Basin (van Hauen, Degerböls and Trold Fiord formations; Beauchamp et al., 2009). The uppermost fossiliferous carbonate unit in the Kapp Starostin Formation occurs ~40 m below the contact with the overlying uppermost Permian-Lower Triassic Vardebukta Formation. The topmost part of the Kapp Starostin Formation is dominated by spiculitic chert, an interval that is in part Late Permian in age (Blomeier et al., 2013) and considered equivalent to the Black Stripe and Lindström formations of the Sverdrup Basin (Beauchamp et al., 2009).

The Vardebukta Formation is a unit of shale, siltstone and minor sandstone that is devoid of carbonate and chert. The formation is mostly Early Triassic (Griesbachian–Dienerian) in age as shown by ammonoid and conodont fauna (Mørk et al., 1982; Nakrem et al., 2008; Tozer and

Parker, 1968). While the contact between the Kapp Starostin and Vardebukta formations was for many years considered the Permian-Triassic Boundary (PTB) (e.g. Mørk et al., 1982; Mangerud and Konieczny, 1993), it is now widely accepted that the basal beds of the Vardebukta Formation are latest Permian (Changhsingian) in age. While *Hindeodus parvus* – the globally recognized fossil for the base Triassic as documented at the PTB GSSP at Meishan, China (Yin et al., 2001) – has yet to be recovered in the basal Vardebukta Formation at Festningen, chemostratigraphic considerations have led Wignall et al. (1998) to place the P-T boundary ~6 m above the Kapp Starostin-Vardebukta contact based on the stratigraphic position of the globally-recognized $\delta^{13}C$ minimum, a practice since followed by others (e.g. Dustira et al., 2013). In the Sverdrup Basin, *H. parvus* was recovered 31.75 m above the base of the Blind Fiord Formation – the stratigraphic and lithological equivalent to the Vardebukta Formation – at the Otto Fiord South section on NW Ellesmere Island (Henderson and Baud, 1997), while at West Blind Fiord, SW Ellesmere Island, the PTB is believed to occur ~ 12.5 m above the base of the Blind Fiord Formation (Algeo et al., 2012), based on the presence *of Clarkina taylorae* which occurs higher up in the section; *C. taylorae* is considered concurrent with *H. parvus.* At both Sverdrup localities, typical late Changhsingian conodonts have been recovered from the basal few meters of the Blind Fiord Formation (Henderson and Baud, 1997; Beauchamp et al., 2009; Algeo et al., 2012).

Wignall et al. (1998) show a stepwise loss of fauna at Festningen as summarized here. The majority of carbonate secreting taxa was lost ~12 m below the top of the Kapp Starostin Formation. The brachiopod fauna present in the upper-most beds may represent an early to late Lopingian age (Nakamura et al., 1987). After loss of carbonate fauna, siliceous sponges were the only taxa that remained abundant to the top of the formation. However, ichnofabrics indicating the persistent presence of soft-bodied fauna are also abundant. The top of the Kapp Starostin

Formation coincides with the loss of siliceous sponges and an abrupt change in ichnofabrics, marked by disappearance of *Zoophycus* and *Chondrite*s. The basal 5 m of the Vardebukta Formation is characterised by *Planolites* and pyritized small burrows, above which sediments become finely laminated and lacking in trace fossils.

Change is also observed in the terrestrial environment as indicated by palynological assemblages at Festningen (Mangerud and Konieczny, 1993). The upper-most Kapp Starostin Formation is dominated by a variety of pollen and spores from gymnosperms (conifers, pteridosperms, and rare cordaites) and pteridophytes. Basal rocks of the overlying Vardebukta Formation contain an overall lower diversity of palynomorphs than observed in the Kapp Starostin Formation with the exception that spores of lycopsids and bryophytes are present with greater diversity than observed in underlying strata. Pollen of gymnosperms are represented by *Lunatisporites* spp., a spore with pteridosperm affinity, and the first appearance of *Tympanicysta stoschiana* occurs in the basal Vardebukta Formation. Acritarchs (*Veryhachium* spp. and *Micrhystridium* spp.) then recover and become abundant in the Vardebukta Formation (Mangerud and Konieczny, 1993).

Acritarchs may have constituted the pioneering taxa of the planktonic oceanic realm following marine perturbation associated with the latest Permian event. Oceanic conditions may have been favourable for the development of widespread acritarch and prasinophyte blooms due to stratified ocean waters and elevated atmospheric carbon dioxide concentrations associated with volcanic activity and/or extreme oligotrophy in the mixed layer due to slow oceanic circulation (Martin, 1996; Payne and van de Schootbrugge, 2007).

3.0 METHODS

3.1 Sample Collection

Sampling was conducted at 50 cm spacing, from 20 to 4 m below the top of the Kapp Starostin Formation, and then across the LPE interval sample spacing was reduced to 20 cm, from 4 m below to 18 m above the formation contact. Sample spacing is reported in metres above (positive) and below (negative) the last chert bed that defines the top of the Kapp Starostin Formation. A total of 93 samples are included in this study.

In the field, weathered surfaces were removed and samples were collected from a narrow defined zone no greater than 2 cm thick. In the laboratory any remaining weathered surfaces were removed and fresh samples were powdered using an agate mortar and pestle and split into sub-samples for subsequent analyses.

3.2 Geochemistry

Total organic carbon (TOC) was measured using Rock-Eval 6©, with ± 5% analytical error of reported value, based on repeats and reproducibility of standards run after every 5th sample (Lafargue et al., 1998). Total sulphur (TS) and total carbon (TC) was measured on a LECO 444 analyzer, with the average of 3 repeat measurements reported, with ± 2% analytical error. Total inorganic carbon (TIC) was calculated from (TIC=TC-TOC). Elemental determinations were conducted on powdered samples digested in a 2:2:1:1 acid solution of H_2O-HF-$HClO_4$-HNO_3, and subsequently analyzed using a PerkinElmer Elan 9000 mass spectrometer, with ± 2% analytical error. Hg was measured at GSC-Atlantic by LECO® AMA254 mercury analyzer (Hall and Pelchat, 1997) (± 10%).

3.3 Stable Isotope analyses

Stable isotope measurements were conducted at the Isotope Science Laboratory, University of Calgary. For determination of $\delta^{13}C_{org}$, samples were washed with hydrochloric acid, and rinsed with hot distilled water to remove any carbonate before determination of $\delta^{13}C$ of organic carbon. $\delta^{13}C$ and $\delta^{15}N$ were measured using Continuous Flow-Elemental Analysis-Isotope Ratio Mass Spectrometry, with a Finnigan Mat Delta+XL mass spectrometer interfaced with a Costech 4010 elemental analyzer. Standards were run every 5th sample. Combined analytical and sampling error for $\delta^{13}C_{org}$ and $\delta^{15}N_{org}$ is ± 0.2‰.

3.4 Absolute age dating

Zircons were separated from bentonite layers using conventional heavy liquid and magnetic techniques at Curtin University, Perth (Australia). Zircon grains were handpicked under a binocular microscope. Together with standards BR266 (Stern, 2001) and OGC-1 (Stern et al., 2009) and NIST NBS610 glass, these zircons were mounted in 25 mm diameter epoxy disc and then polished and coated with gold.

Zircons were imaged using Cathodoluminescence (CL) techniques on a Zeiss 1555 VP-FESEM in the Centre for Microscopy, Characterisation and Analysis of the University of Western Australia. Zircon analyses were performed on the SHRIMP II at the John de Laeter Centre for Isotope Research, Curtin University, and followed standard operation procedures (Compston et al., 1984; Williams, 1998). The primary (O_2^-) ion beam was 0.7 nA on a 15 µm spot. The data were processed using the SQUID and ISOPLOT program (Ludwig, 2003; Ludwig, 2009). Common

Pb was subtracted from the measured compositions using the measured ^{204}Pb and a common Pb composition from the model of (Stacey and Kramers, 1975) at the appropriate stage of each analysis.

4.0 RESULTS

4.1 Absolute Age Dating

Two previously unreported bentonite layers ~2 cm thick were found in the basal Vardebukta Formation, 2.6 and 13 m above the top of the Kapp Starostin Formation (hereafter referred to as ash layer). The layers were isolated and collected in the field. Zircons were only recovered from the lower layer at 2.6 m above the formation boundary. The zircon grains are inclusion-free bipyramidal prisms that are sometimes slightly rounded. These grains range in length from 60 μm to 100 μm, and are light brown and occasionally light pink. The CL imaging shows uniform zircons with typical oscillatory zoning and composite zircons with cores overgrown by thin rims (Fig. 3a).

Twenty one analyses were performed on thirteen zircons. Age data are presented in Table 1 with 1σ precisions. Six of the 21 analyses were rejected due to the high common lead, and sixteen analyses yielded concordant or nearly concordant ages ranging from 244 Ma to 2685 Ma (Fig. 3b). Ten concordant or nearly concordant analyses plot in one single population with a weighted mean $^{206}Pb/^{238}U$ age of 252 ± 3 Ma (MSWD = 0.92) (Fig. 3b). There are also six older ages: two Late Silurian-Early Devonian (412 ± 8, 428 ± 8 Ma), and four Neoarchean (2645 ± 6, 2663 ± 17, 2642 ± 12 and 2685 ± 4 Ma).

4.2 Carbon isotope records

Given the lack of carbonates, the organic carbon isotope record was examined at the Festningen section. At 15 m above the Kapp Starostin Formation contact, shales show visible signs of thermal alteration from an overlying Cretaceous sill which starts at ~19 m. Thermal effects can also be observed in the geochemical record close to the sill itself, although there is no apparent impact on the key part of the section in the basal 15 m of the Vardebukta Formation (Fig. 4). Rock-Eval 6© results in the basal 15 m provide an average Tmax value of 453 °C, indicating that organic matter in the shales are not thermally affected by the overlying sill, and that away from the localised thermal affects, the Festningen section has never been heated past the upper end of the oil window (note Tmax values reflect relative, not actual, burial temperatures). At the equivalent maximum burial temperatures, the stable isotope values of organic carbon are not altered (Hayes et al., 1983). The Oxygen Index derived from RockEval analyses has an average value of 28, consistent with well-preserved organic matter.

The $\delta^{13}C$ record of the organic carbon shows two initial minor negative shifts of 1 to 2‰ at -12 m (where calcareous shelly macrofauna are lost), and then again at 3 m below the top of the Kapp Starostin Formation (Fig. 4a, Table 2). There is a brief positive shift in $\delta^{13}C$-values just below the Kapp Starostin/Vardebukta contact. The top of the Kapp Starostin Formation is marked by onset of a progressive ~8‰ negative shift in $\delta^{13}C$, over the basal 5 m of the Vardebukta Formation, to a low of -33‰. This $\delta^{13}C$ low is coincident with the level where bioturbation disappears (Wignall, 1998). The $\delta^{13}C$ values then remain relatively stable for the next 10 m, after which there are thermal affects due to the overlying sill (Fig. 4).

Overall organic carbon content is low, with values less than 0.8% TOC throughout the studied interval (Fig. 4b). In the interval from 20 to 12 m below the top of the Kapp Starostin

Formation, TOC values vary around 0.5 to 0.6%. TOC values then drop at the level associated with loss of calcareous macrofauna (~12 m below the top of the Kapp Starostin Formation) to values around 0.4%. The TOC remains at these values for the remaining 12 m of the Kapp Starostin Formation. Above the Kapp Starostin Formation, there is a progressive drop in TOC associated with the drop in $\delta^{13}C_{org}$ values until the first ash layer at 2.6 m, where there is an abrupt increase in TOC to values of 0.5 % above this level. TOC then fluctuates for the rest of the section, with peak values of 1.03% at 8.2 m above the formation contact.

The TIC record is also plotted in Figure 4c. Even in the basal part of the section, where carbonate fossils are observed, TIC is still low (~0.5 %). Above the loss of shelly macrofauna TIC values drop to <0.1% for the remainder of the Kapp Starostin Formation. Above the formation contact, there is a progressive increase in TIC over the zone where $\delta^{13}C_{org}$ values drop, to values of ~1%. The TIC values then remain relatively constant until the zone of thermal influence where they drop again. The one exception is peak values >2.5% around 8 m above the formation contact, coincident with a zone of peak TOC values (Fig. 4).

4.3 Redox Proxies

Several trace elements have been shown to be useful proxies for marine redox state (Mo, U, V) in addition to pyrite associated Fe (Fepy) (Scott and Lyons, 2012; Tribovillard et al., 2006). The variation of these proxy elements are plotted in Figure 5. Fepy values are consistently low (< 0.5 %) in the upper Kapp Starostin Formation, through the zone of the last carbonate producers, and across the formation boundary as marked by the loss of sponges (Fig. 5a). Pyrite is rare until above the first ash layer at 2.6 m above the formation contact, after which there is a significant increase in Fepy, to values above 1%. This increase in pyrite is seen also in a plot of TS versus

TOC (Fig. 6a). Here samples below the ash bed from both the Kapp Starostin and Vardebukta formations plot close to the oxic/sub oxic boundary as defined for ancient sediments (Raiswell and Berner, 1985). Samples above the ash layer show significantly higher Fepy values, with peak levels in the finely laminated black shale at ~ 8 m above the Formation contact (Fig. 5a). In general, Fepy values show inverse trends to $\delta^{13}C_{org}$ (Fig. 6b) across the boundary.

The Mo concentrations in the Kapp Starostin and the basal Vardebukta formations (solid circles in Fig. 5b) are consistently lower than average marine shale values, relative to Post-Archean average Australian shale (PAAS) (Taylor and McLennan, 1985). However, Mo values increase to > 20 ppm within a narrow interval of the laminated black shale at ~ 8 m above the Kapp Starostin Formation (Figs. 2b,c; 5b). A similar trend is observed in U and V data (solid circles in Figs. 5c,d). Through the upper Kapp Starostin Formation and basal Vardebukta Formation, U and V concentrations are consistently below average marine values (except peaks associated with the first ash layer). While there is an initial minor increase at the Kapp Starostin/ Vardebukta contact, values do not consistently exceed average marine shale until after the level where burrowing organisms are lost (~5 m above the formation contact). The U and V concentrations peak in the same laminated black shale ~8 m above the formation contact, where Mo and TOC values are also highest.

Given the change from chert to shale at the formation boundary, redox sensitive elements were also normalised to Al to account for potential lithologic affects (dashed lines in Fig. 5). As with absolute values, Al normalised values show a decline (Mo, U) in the lower Vardebukta Formation, or remain at low values (V) relative to the underlying Kapp Starostin Formation chert. The only significant increase in the metal/Al ratio is associated with the laminated black shale interval at 8 m above the formation contact.

4.4 Trace Metals

The variability of trace metals (Cu, Pb, As, Co, Ni, Hg) is illustrated in Figure 7. Absolute concentrations are plotted (dots) along with values normalized to Al (lines) to account for potential lithologic changes. Mercury deposition over geologic time is strongly controlled by organic matter (Grasby et al., 2013b), and therefore anomalous Hg deposition is best observed by normalizing relative to TOC (Sanei et al., 2012). Similarly, Ni is strongly scavenged by organic matter (Tribovillard et al., 2006) and is also normalized relative to TOC. Trace metal values in the lowest chert dominated portion of the section are relatively constant and below PAAS values (vertical dotted lines in Fig. 7). At 12 m below the formation contact, where the section is marked by the final disappearance of calcareous macrofauna, there is a small but distinct shift to lower values of all metals as it transitions from shaly chert to pure chert. However, there is no notable shift in normalized values at this level. The metals (concentrations and ratios) remain at low levels through to the top of the Kapp Starostin Formation. In the basal 5 m of the Vardebukta Formation there is a significant increase in all trace metals, to values well above PAAS. This increase is also observed in the Al normalized values. The Ni/TOC and Hg/TOC ratios also show a significant spike at in the basal Vardebukta Formation. After this trace metal spike, there is a gradual decline to values near or below PAAS. One exception is a brief increase associate with a zone defined by high Mo values ~ 8 m above the formation contact, where there is also a peak in TOC values (Fig. 7). In general, trace metals in the basal Vardebukta Formation show much greater variability than in the upper portion of the Kapp Starostin Formation.

4.5 Nitrogen Isotopes

The $\delta^{15}N$ of total nitrogen has been used to assess changes in nutrient cycles across the LPE (Knies et al., 2013; Schoepfer et al., 2013). Major changes in nutrient cycling, through shifts in denitrification and/or atmospheric nitrogen fixation can strongly influence the $\delta^{15}N$ signal of the marine nitrate pool. For the levels of thermal maturity found in the Festningen section, there are negligible effects on the stable isotope values of N (Ader et al., 1998; Bebout and Fogel, 1992). The $\delta^{15}N$ values of total N are illustrated in (Fig. 4d). Results show that through the Kapp Starostin that $\delta^{15}N$ values are consistently around 7‰. There is then a progressive decline in $\delta^{15}N$ values through the basal 5 m of the Vardebukta Formation until the level at which bioturbation was lost. Above the level where bioturbation is lost, values remain consistently around 5‰.

4.6 Chemical Index of Alteration

The Chemical Index of Alteration (Sydeman et al.) (Nesbitt and Young, 1982) provides a proxy for the degree of chemical weathering as recorded in siliciclastic sedimentary rocks whereby increased chemical weathering mobilizes Na, K, and Ca during the transformation of feldspar minerals to clays. However, the CIA index needs to corrected for potential Ca from inorganic carbon (Fedo et al., 1995). For Festningen, the CIA index shows almost no variation through the section analyzed, with values consistently near 80 (Fig. 4e). Towards the top of the section the CIA values drop within the zone of thermal influence.

5.0 DISCUSSION

5.1 Age dating

The bentonite layer 2.6 m above the top of the Kapp Starostin Formation had one dominant population with a weighted mean age of 252 ± 3 Ma, which we interpreted as the crystallisation age of the volcanic ash. Six older ages were obtained in zircons which are slightly rounded and likely represent xenocryts (Fig. 3b). The source of these older ages may be: 1) Silurian to Early Devonian granites, located in the Nordaustlandet Terrane of northeast Svalbard whose ages range from 410 to 440 Ma (Johansson et al., 2002); and 2) a Neoarchean quartz-monzonite, located in the Ny-Friesland, northern Svalbard, which yielded an upper intercept of 2709 ± 28 Ma, considered the best estimate of the crystallisation age (Hellman et al., 2001).

5.2 Carbon isotope records and the LPE Boundary

While not having sufficient precision to be definitive, the 252 Ma age of the ash layer suggests that the top of the Kapp Starostin Formation represents the global LPE boundary. This is further constrained by carbon isotope data. The organic carbon isotope record at Festningen shows a distinct negative $\delta^{13}C$ excursion initiated at the basal most Vardebukta Formation (Fig. 4), consistent with negative excursions associated with the LPE horizon observed in inorganic carbon isotope records (Korte and Kozur, 2010). This negative carbon isotope shift is also consistent with organic carbon isotope records from other boreal settings (e.g. Sverdrup Basin - Grasby and Beauchamp (2008;2009)); NE British Columbia - (Wang et al., 1994; Wignall and Newton, 2003), East Greenland (Twitchett et al., 2001); and Norway/Spitsbergen (Dustira et al., 2013; Hermann et al., 2010). In their review, (Korte and Kozur, 2010) showed that the initial negative decline in $\delta^{13}C$ values started at the LPE and reached a minimum $\delta^{13}C$ value after the extinction event. (Shen et al., 2011) also show that the negative excursion in the carbon isotope record occurs after the main extinction event in the Tethys. As well, at Meishan (Burgess et al., 2014) show that after the initial negative peak, the broad decline in $\delta^{13}C$ values occurs after the main extinction event. Therefore, we interpret the negative shift at Festningen as being consistent with the global pattern for the negative carbon isotope excursion initiating at the LPE event. Based on this interpretation, we follow previous workers who used the $\delta^{13}C$ minimum as the approximate P/T boundary in Spitsbergen (Dustira et al., 2013; Wignall et al., 1998), and the onset of the major $\delta^{13}C$ decline above the last chert beds to mark the LPE horizon. This makes the LPE horizon coincident with the top of the Kapp Starostin Formation, that also marks the loss of sponges as well as collapse of well-developed ichnofauna, including *Zoophycus* and *Nereites* (Wignall et al., 1998).

The tops of the Kapp Starostin Formation also marks a shift in palynological assemblages, from those dominated by gymnosperms to an assemblage dominated by lycopsids, as described at Festningen and other sections on Spitsbergen (Mangerud and Konieczny, 1993). This lycopsid "spore peak" in latest Permian strata is well documented elsewhere in the northern hemisphere (Hochuli et al., 2010; Twitchett et al., 2001). These changes in palynoassemblages across the boundary represent major vegetation community collapse of Late Permian gymnosperm-dominated ecosystems followed by re-colonization by pioneering lycopsids and bryophytes and components of typical Early Triassic shrubland communities (Hochuli et al., 2010; Twitchett et al., 2001), representing a terrestrial response to environmental stress followed by rapid, but short lived, recovery. (Twitchett et al., 2001) noted that the synchronous collapse of the marine and terrestrial ecosystem preceded a sharp negative carbon isotope excursion at the LPE boundary in East Greenland. As well, (Hermann et al., 2010) showed that in the Trøndelag and Finnmark Platform, Norway, the marine extinction level was immediately followed by the increase in spore abundance and a sudden drop of C-isotope values. Thus, the Latest Permian terrestrial collapse observed across NW Pangea is coincident with the marine extinction marked by the loss of chert forming siliceous sponges.

The loss of chert was a global feature at the LPE (Beauchamp and Baud, 2002; Beauchamp and Grasby, 2012) that has been correlated with the extinction event in Meishan (Wignall and Newton, 2003) and onset of the Early Triassic Chert Gap. While driven by sponge extinction it may also represent a significant drop in silica solubility due to significant increase in ocean temperatures (Beauchamp and Grasby, 2012; Joachimski et al., 2012). Previous workers also place the LPE boundary at the top of the last chert beds in correlative strata from the Sverdrup Basin (Embry and Beauchamp, 2008; Grasby and Beauchamp, 2008; Proemse et al., 2013) and western Canada (Schoepfer et al., 2013). However, this placement of the LPE boundary contrasts with the claims of (Algeo et al., 2012) who speculated that that the loss of sponges and complex ichnofabric represents an earlier extinction than the LPE event itself (their "arctic event"). The level that they assign as the LPE horizon at the West Blind Fiord section of the Sverdrup Basin is marked by minor geochemical changes in the overlying shales (Fig. 8). These are more consistent with those observed in Festningen at the level of the first ash bed. The samples that (Algeo et al., 2012) analyzed from this level at WBF (collected by two of us, S.G. and B.B.) were in fact ash layers and thus the chemistry is not representative of marine conditions as they assumed.

5.3 Redox Proxies

Multiple proxies for anoxia examined as part of this work, including redox sensitive trace elements, Fe_{py}, and TC/TC, show similar trends. In the chert-dominated upper Kapp Starostin Formation redox sensitive elements are consistently lower than average PAAS values, and

TS/TOC values plot along the oxic boundary for oxic/suboxic waters. Above the Kapp Starostin there is a slight shift to higher concentrations of redox sensitive elements, however they remain below PAAS values, suggesting a largely oxic system in the basal 2.6 m of the Vardebukta Formation. Such an oxic environment is consistent with Fe_{py} that remain low through the Kapp Starostin and basal Vardebukta formations. These data suggest then that the LPE boundary, marked by the loss of siliceous sponges, occurs under oxic to dysoxic conditions at Festningen.

Above the first ash layer at 2.6 m TS values increase and Fepy values plot in the sub-oxic zone of Raiswell and Berner (1985). The peak values of redox sensitive elements, exceeding PAAS, as well as peaks in Al normalized values occurs at ~ 8 m in association with the black laminated shale above the zone were burrowers are lost. These increased concentrations of redox sensitive elements, both absolute and normalized to Al are strong indicators of marine anoxia (Tribovillard et al., 2006), suggesting that conditions at Festningen transitioned to a more anoxic environment after the LPE extinction boundary. This is supported by the progressive shift to lower $\delta^{15}N$ values that suggests increased fixation of atmospheric N_2, possibly in response to increasing anoxia (Schoepfer et al., 2013; Proemse et al., 2013; Knies et al., 2013). This interpretation of anoxia is consistent with original work by Wignall et al. (1998) who suggested onset of anoxia at this level, in addition to recent work by (Bond and Wignall, 2010) who showed pyrite framboid data at Festningen consistent with transition to anoxic conditions at the same level.

5.4 Trace metals

A key aspect of the Festningen section is the significant increase in metals at the LPE boundary that occurs at a level where anoxia has not yet developed. In fact, metal concentrations right above the LPE are greater than when anoxic conditions eventually develop higher in the section. These high metal concentrations argue against these anomalous metal loads being associated with increased drawdown into sediment. Previously it has been suggested that metal enrichments at the LPE boundary could be related to high loading rates from the Siberian Trap eruptions (Grasby et al., 2011, Sanei et al., 2012). Similarly, we interpret the anomalous metal concentrations at the LPE boundary, both absolute and Al normalized, to be related to enhanced metal flux from the Siberian Traps. While described here for Festningen, similar trace metal spikes have been observed in the Sverdrup Basin (Grasby et al., 2011) as well as at Meishan, where Ni concentrations show a significant increase just prior to the carbon isotope shift (Kaiho et al., 2001; Rothman et al., 2014), implying that increased metal loading at the LPE is a global phenomenon.

6.0 Progressive environmental deterioration

Results from our Festningen study demonstrate evidence for progressive environmental deterioration leading up to and across the LPE event. This can be characterised by three main events: 1) lysocline shoaling driving loss of carbonate producers, 2) volcanic metal loading related to volcanics, and 3) onset of anoxia.

6.1 Loss of Carbonate Producers

The first notable event in the Festningen section is the loss of carbonate producers (i.e. brachiopods, bivalves, corals, bryozoans, foraminifers) around 12 m below the top of the Kapp Starostin Formation (Wignall et al., 1998); marking the last appearance of any carbonate secreting organisms prior to the LPE event. Not only are carbonate fossils absent after this point, but TIC values drop to near zero (Fig. 4), indicating a complete absence of carbonate sediment. The loss of carbonate producers is also marked by a small negative shift in $\delta^{13}C$ and drop in TOC (Fig. 4).

Early work had interpreted the loss of carbonate producers as being driven by a shift to cooler water temperatures (Beauchamp and Baud, 2002; Reid et al., 2007; Stemmerik and Worsley, 1995). However, reduced ocean temperatures are insufficient to account for loss of carbonate production in clastic-starved, well-lit, aerobic environments (Beauchamp and Grasby, 2012). As well, temperatures in the Boreal Realm were already increasing during latest Permian time (Beauchamp and Grasby, 2012) when silica producers became the dominant sediment producer. Instead, the transition from carbonate to silica factories most likely relates to lysocline shoaling driven by increasing atmospheric CO_2 (Beauchamp and Grasby, 2012). Carbon cycle modelling suggests progressive increase in atmospheric CO_2 through the Late Permian (Berner, 2006) with values as high as 4000 ppm prior to the LPE (Cui and Kump, 2014). Given the inverse solubility of $CaCO_3$ with temperature, high latitudes would be most susceptible to increasing atmospheric CO_2 levels, becoming understaturated with respect to carbonates, while lower latitudes maintained shallow water carbonate factories.

6.2 Metal loading

The eruption of the Siberian Traps, which roughly coincides with the LPE extinction (Burgess et al., 2014), could have had both positive and negative impact on global ecosystems through release of both nutrients and toxic metals (Frogner Kockum et al., 2006; Hoffmann et al., 2012; Jones and Gislason, 2008). Metal loading from volcanic eruptions can serve as a significant input of limiting nutrients (e.g. Fe, Ni: (Boyd et al., 2000; Konhauser et al., 2009; Langmann et al., 2010), increasing primary productivity, that may relate to microbial blooms which occur at the LPE (Lehrmann, 1999; Xie et al., 2010; Xie et al., 2005). At the same time, high rates of metal loading could exert a toxic shock to both the marine and terrestrial system. While increased acid rain related to the Siberian Trap eruptions has been argued to have significant impact on the terrestrial environment (Black et al., 2014), metal loading would also be deleterious as it dramatically decreases photosynthetic efficiency in vascular plants (Odasz-Albrigtsen et al., 2000). Although there is pollen evidence for significant impact to the terrestrial system, CIA does not change across the boundary, indicating no significant changes in chemical weathering rates as suggested for lower latitudes (Sephton et al., 2005; Sheldon, 2006). This is consistent with (Hochuli et al., 2010) who show a rapid recovery of plant ecosystems from records in the southern Barents Sea, and suggests that in the Boreal realm terrestrial impact was relatively short term.

Volcanic eruptions are associated with release of metals to the atmosphere (Vie le Sage, 1983), that can form significant components of global element cycles (e.g. volcanoes account for 40% of the modern natural component of the global Hg budget (Pyle and Mather, 2003). Volatile metals released from the magma (e.g Cu, Zn, Ni, Pb, Cd, Hg, As) can form stable compounds (e.g. $CdCl_g$, CdS_g, (Symonds et al., 1987)) that condense onto ash particles, creating notable metal enrichments in ash relative to the source magma (Bagnato et al., 2013). Leaching experiments of ash fall show significant subsequent release of these metals into water (Olsson et al., 2013; Ruggieri et al., 2011). Whether the resultant dissolved concentrations can be significant enough to create toxicity, or in some cases nutrient influx (e.g. Fe), would be a function of the ash loading rate (Olsson et al., 2013). In any case, ash loading would represent an anomalous metal load to a system that can be used as a proxy for enhanced volcanic activity in the geologic record (Grasby et al., 2011; Grasby et al., 2013b; Sanei et al., 2012; Sial et al., 2013; Silva et al., 2013).

The Siberian Traps also intruded trough the Tunguska sedimentary basin, and it has been suggested that this induced combustion of coal and organic rich shales, causing release of over 3 trillion tons of carbon (Grasby et al., 2011; Korte et al., 2010; Ogden and Sleep, 2012; Reichow et al., 2009; Retallack and Jahren, 2008; Saunders and Reichow, 2009; Svensen et al., 2009). As with volcanoes, volatile metals released during combustion (e.g., Be, Zn, As, Cd, Tl, Pb, and U) condense and concentrate onto the resulting fly ash that is composed dominantly of SiO_2, Al_2O_3 and Fe_2O_3 particles (Gieré et al., 2003). Enrichment factor of metals, relative to the source organics, can range from 30x up to 100x (Gieré et al., 2003; Klein et al., 1975; Papastefanou, 2010). Similar concentration of metals onto fly ash has been observed during combustion of oil shales (Blinova et al., 2012). Metal enrichment is much greater in the smaller size fraction, as they have the largest surface area for condensation of volatiles per unit mass (Davison et al., 1974; Furuya et al., 1987; Kaakinen et al., 1975b; Martinez-Tarazona and Spears, 1996; Smith et al., 1979). The smallest size fraction also has the longest atmospheric residence times, and consequently the greatest spatial distribution during atmospheric transport (Kaakinen et al., 1975a; Smith et al., 1979). Similar to volcanic ash, metals condensed onto the surface of fly ash particles are also released when ash is submerged in water (Bednar et al., 2010). Evidence for coal ash loading and metal release at the LPE was observed in the Sverdrup Basin by Grasby et al. (2011), suggesting that coal ash dispersal was widespread in the northern hemisphere during the latest Permian.

The largest volcanic eruption in Earth history, the Siberian Traps, combined with combustion of organics in the Tunguska Basin, would have had an extremely high metal loading rate that far exceeds normal background. As an example (Sanei et al., 2012) calculated a Hg loading rates from the Siberian Traps that would be 4x above modern anthropogenic emissions, assuming a 500 ky eruption period. Similar estimates for other metal fluxes can be made based on the metal/S ratio for modern volcanic emissions (Nriagu, 1989), and estimates of total SO_2 release of 3.8×10^{13} Mg from the Siberia Trap eruptions (Beerling et al., 2007). Averaged over an assumed maximum 500 ky eruption history gives a conservative minimum increase. Based on this, Siberian Trap eruptions may have increased global metal flux to the atmosphere from 9% (Se) to 78% (Co) above modern natural background flux (Mather et al., 2013; Nriagu, 1989) (Table 3). However, Siberian Trap magmatism was more likely episodic over the total eruption interval (Pavlov et al., 2011). Such episodic eruption would mean that rather than an overall average background increase, the extinction interval would be better characterized by pulses of extreme metal loading, significantly higher than those estimated here. Pavlov et al. (2011) estimated that the total eruption intervals may represent as low as 8% of the total eruption history (suggesting a net ~40 ky for metal release). Based on this, metal flux by the Siberian Traps may have ranged from 107% (Se) to 977% (Co) above background.

While estimates of metal loading rates related to the Siberian Trap contain uncertainties, it is interesting to note that even conservative estimates are of the same order of magnitude as modern anthropogenic metal release (Pacyna and Pacyna, 2001) that are subject of global concern. Whereas, higher rates based on a more likely pulsed eruption history are one to two orders of magnitude greater than modern anthropogenic emissions. Such extreme loading rates may readily explain the metal anomalies at the LPE boundary, and likely represented a toxic shock to both marine and terrestrial ecosystems.

6.3 Anoxia

Our study suggests that the main LPE horizon at Festningen occurs under oxic to dysoxic conditions, but that anoxia developed soon after and is associated with a final extinction of benthic life. There have been suggestions that the initial extinction event occurred under at least local, and perhaps regional, oxic conditions in other NW Pangean (Algeo et al., 2010; Knies et al., 2013; Proemse et al., 2013) and Neotethyan locations (Korte et al., 2004; Loope et al., 2013; Richoz et al., 2010). However, such conditions are often only encountered in shallower proximal settings. In the somewhat more distal setting of Tschermakfjellet, 60 km to the northwest of Festningen, the redox record indicates the gradual onset of oxygen-restricted deposition in the upper Kapp Starostin Formation (Dustira et al. 2013), whereas dysoxia is not seen in the shallower Festningen section until the latest Perminan in the lower Vardebukta Formation. Similarly, in the Sverdrup Basin Proemse et al. (2013) show at the LPE a strongly developed oxygen minimum zone with euxinic conditions in deep water settings and oxic shallow water environments. This suggests a gradual expansion of dysoxic bottom waters into shallow water environments (Grasby et al., 2009; Proemse et al, 2013). It is during this expansion phase that the LPE occurs, even in locations like Festningen where oxic waters remained. As the habitable seafloor area shrank, the additional stress caused by intense trace metal poisoning may have driven the extinction of the low pH-tolerant benthos of NW Pangea. This relative timing of anoxia is consistent with paleo-marine temperature records that show rapid warming of global oceans (which would drive enhanced anoxia) occurred after the main extinction event (Joachimski et al., 2012; Sun et al., 2012). This may imply then that the initial eruption of the Siberian Traps had an initial short tern toxic metal loading effect of global ecosystems that was followed by a delayed rapid global warming related to emissions of greenhouse gases (Dustira et al., 2013; Grasby and Beauchamp, 2009).

7.0 Summary and Conclusions

The Festningen section shows a remarkable record of progressive environmental deterioration through latest Permian time. Three major steps are observed, which we interpret as reflecting progressive ecological damage. First there was the gradual lysocline shoaling along the NW margin of Pangea leading to the final loss of carbonate producers at 12 m below the top of the Kapp Starostin Formation. Such loss of carbonate producers has been recorded over much of NW Pangea, where carbonate factories contracted into increasingly narrow mid to inner shelf areas throughout the Middle Permian, and were nearly eradicated by Late Permian time except for nearshore environments (Beauchamp and Grasby, 2012; Bugge et al., 1995; Ehrenberg et al., 2001; Gates et al., 2004). While these carbonate factories were lost, silica productivity was maintained with the result that the nearshore siliceous limestones were replaced by across-the-shelf spiculites (Beauchamp and Baud, 2002; Beauchamp and Desrochers, 1997; Beauchamp and Grasby, 2012). This Lysocline shoaling would reflect a gradual process related to long term changes in atmospheric CO_2, that was most strongly manifest along the NW margin of Pangea in Late Permian time. However such affects would not be expressed at low latitude shelves in the Tethys that maintained productive carbonate factories.

If correct, evidence for lysocline shoaling suggests that the Late Permian oceans were under progressive increasing stress of marine systems leading up to the LPE event. Although, even if the loss of carbonate producers may reflect a progressive shift to a more stressed marine environment, siliceous sponges were able to still thrive and diverse bioturbators continued to produce a pervasively burrowed fabric.

The second major environmental impact is recorded at the LPE event itself, when the loss of sponges and major loss of burrowing organisms occurs during oxic conditions. We argue that high metal loading rates at this time reflects onset of massive eruption of the Siberian traps and associated volatile and toxic element release to the global atmosphere. Although burrowing animals still survived, trace fossils became limited to *Planolites* and small burrows (Wignall et al., 1998). Coincidental with the marine LPE, pollen records at this time indicate dramatic shifts to highly stressed terrestrial environments, that implies simultaneous collapse of both marine and terrestrial systems.

The third major impact oobserved at Festningen is a distinct shift to anoxia 2.6 m above the LPE horizon, associated with a distinct loss of remaining burrowers. We suggest that development of anoxia provided the third and final blow to the survivors. The continued spread of anoxia could have several causes. Rapid increasing sea temperatures occurred just after the main extinction that would have decreased oxygen solubility (Romano et al., 2013; Sun et al., 2012), and could have also driven release of any remaining deep-marine gas hydrates, which would also consume dissolved oxygen in marine waters (Majorowicz, et al., 2014; Ruppel, 2011).

Results from this study show a remarkable record of environmental deterioration associated with the LPE event that struck progressively down ecologic systems, and demonstrates the need for high resolution studies to characterize the nature of rapid change in global biogeochemical cycles during this dramatic period of Earth history.

Acknowledgements

The Norwegian Polar Institute provided logistical support. SEM imaging was carried out in the Centre for Microscopy and Microanalysis at the University of Western Australia, which is funded by the University and the Western Australian and Australian Governments. Zircon analyses were conducted using the SHRIMP-II ion microprobe of the John de Laeter Centre for Isotope Research at Curtin University, Perth, Australia, operated by a WA university-government consortium with ARC support. Reviews from Matthew Clapham and an anonymous reviewer are greatly appreciated. This research was made possible by the Bundesanstalt für Geowissenschaftern und Rohstoffe, Geozentrum, the Natural Science and Engineering Research Council of Canada, and the Geological Survey of Canada (Contribution xxxx).

References

Ader, M., Boudou, J.-P., Javoy, M., Goffe, B., and Daniels, E., 1998, Isotope study on organic nitrogen of Westphalian anthracites from the Western Middle field of Pennsylvania (U.S.A.) and from the Bramsche Massif (Germany): Organic Geochemistry, v. 29, no. 1–3, p. 315-323.

Algeo, T., Henderson, C. M., Ellwood, B., Rowe, H., Elswick, E., Bates, S., Lyons, T., Hower, J. C., Smith, C., Maynard, B., Hays, L. E., Summons, R. E., Fulton, J., and Freeman, K. H., 2012, Evidence for a diachronous Late Permian marine crisis from the Canadian Arctic region: Geological Society of America Bulletin.

Algeo, T. J., Hinnov, L., Moser, J., Maynard, J. B., Elswick, E., Kuwahara, K., and Sano, H., 2010, Changes in productivity and redox conditions in the Panthalassic Ocean during the latest Permian: Geology, v. 38, no. 2, p. 187-190.

Bagnato, E., Aiuppa, A., Bertagnini, A., Bonadonna, C., Cioni, R., Pistolesi, M., Pedone, M., and Hoskuldsson, A., 2013, Scavenging of sulphur, halogens and trace metals by volcanic ash: The 2010 Eyjafjallajökull eruption: Geochimica et Cosmochimica Acta, v. 103, no. 0, p. 138-160.

Beauchamp, B., and Baud, A., 2002, Growth and demise of Permian biogenic chert along Northwest Pangea; evidence for end-Permian collapse of thermohaline circulation Palaeogeography, Palaeoclimatology, Palaeoecology, v. 184, no. 1-2, p. 37-63.

Beauchamp, B., and Desrochers, A., 1997, Permian warm- to very cold carbonates and cherts in northwest Pangea, *in* James, N. P., and Clarke, J., eds., Cool Water Carbonates, Volume 56, SEPM Special Publication p. 327-347.

Beauchamp, B., and Grasby, S. E., 2012, Permian lysocline shoaling and ocean acidification along NW Pangea led to carbonate eradication and chert expansion: Palaeogeography, Palaeoclimatology, Palaeoecology, v. 350-352, p. 73-90.

Beauchamp, B., Henderson, C. M. B., Grasby, S. E., Gates, L., Beatty, T., Utting, J., and James, N. P., 2009, Late Permian sedimentation in the Sverdrup Basin, Canadian Arctic: the

Lindström and Black Stripe formations: Canadian Society of Petroleum Geology Bulletin, v. 57, p. 167-191.

Bebout, G. E., and Fogel, M. L., 1992, Nitrogen-isotope compositions of metasedimentary rocks in the Catalina Schist, California: Implications for metamorphic devolatilization history: Geochimica et Cosmochimica Acta, v. 56, no. 7, p. 2839-2849.

Bednar, A. J., Chappell, M. A., Seiter, J. M., Stanley, J. K., Averett, D. E., Jones, W. T., Pettway, B. A., Kennedy, A. J., Hendrix, S. H., and Steevens, J. A., 2010, Geochemical investigations of metals release from submerged coal fly ash using extended elutriate tests: Chemosphere, v. 81, no. 11, p. 1393–1400.

Beerling, D. J., Harfoot, M., Lomax, B., and Pyle, J. A., 2007, The stability of the stratospheric ozone layer during the end-Permian eruption of the Siberian Traps: Phil. Trans. Royal Society London, v. 365, p. 1843-1866.

Berner, R. A., 2006, Inclusion of the weathering of volcanic rocks in the GEOCARBSULF model: American Journal of Science, v. 306, p. 295-302.

Black, B. A., Elkins-Tanton, L. T., Rowe, M. C., and Peate, I. U., 2012, Magnitude and consequences of volatile release from the Siberian Traps: Earth and Planetary Science Letters, v. 317–318, no. 0, p. 363-373.

Black, B. A., Lamarque, J.-F., Shields, C. A., Elkins-Tanton, L. T., and Kiehl, J. T., 2014, Acid rain and ozone depletion from pulsed Siberian Traps magmatism: Geology, v. 42, no. 1, p. 67-70.

Blinova, I., Bityukova, L., Kasemets, K., Ivask, A., Käkinen, A. c., Kurvet, I., Bondarenko, O., Kanarbik, L., Sihtmäe, M., Aruoja, V., Schvede, H., and Kahru, A., 2012, Environmental hazard of oil shale combustion fly ash: Journal of Hazardous Materials, v. 229-230, p. 192-200.

Blomeier, D., Dustira, A. M., Forke, H., and Scheibner, C., 2013, Facies analysis and depositional environments of a storm-dominated, temperate to cold, mixed siliceous-carbonate ramp: the Permian Kapp Starostin Formation in NE Svalbard: Norwegian Journal of Geology, v. 93, p. 75-98.

Bond, D. P. G., and Wignall, P. B., 2010, Pyrite framboid study of marine Permian–Triassic boundary sections: A complex anoxic event and its relationship to contemporaneous mass extinction: Geological Society of America Bulletin, v. 122, no. 7-8, p. 1265-1279.

Boyd, P. W., Watson, A. J., Law, C. S., Abraham, E. R., Trull, T., Murdoch, R., Bakker, D. C. E., Bowie, A. R., Buesseler, K. O., Chang, H., Charette, M., Croot, P., Downing, K., Frew, R., Gall, M., Hadfield, M., Hall, J., Harvey, M., Jameson, G., LaRoche, J., Liddicoat, M., Ling, R., Maldonado, M. T., McKay, R. M., Nodder, S., Pickmere, S., Pridmore, R., Rintoul, S., Safi, K., Sutton, P., Strzepek, R., Tanneberger, K., Turner, S., Waite, A., and Zeldis, J., 2000, A mesoscale phytoplankton bloom in the polar Southern Ocean stimulated by iron fertilization: Nature, v. 407, no. 6805, p. 695-702.

Bugge, T., Mangerud, G., Elvebakk, G., Mørk, A., Nilsson, I., Fanavoll, S., and Vigran, J. O., 1995, The Upper Paleozoic succession on the Finnmark Platform, Barents Sea. : Norsk Geologisk Tidsskrift, v. 75, p. 3-30.

Burgess, S. D., Bowring, S., and Shen, S.-z., 2014, High-precision timeline for Earth's most severe extinction: Proceedings of the National Academy of Sciences.

Campbell, I. H., Czamanske, G. K., Fedorenko, V. A., Hill, R. I., and Stepanov, V., 1992, Synchronism of the Siberian Traps and the Permian-Triassic Boundary: Science, v. 258, no. 5089, p. 1760-1763.

CASE-Team, 2001, The evolution of theWest Spitsbergen Fold-and-Thrust Belt: Geologisches Jahrbuch, v. B91, p. 733-773.

Compston, W., Williams, I. S., and Meyer, C., 1984, U-Pb geochronology of zircons from lunar breccia 73217 using a sensitive high mass-resolution ion microprobe: Journal of Geophysical Research, v. 89, p. 525-534.

Corfu, F., Polteau, S., Planke, S., Faleide, J. I., Svensen, H., Zayoncheck, A., and Stolbov, N., 2013, U–Pb geochronology of Cretaceous magmatism on Svalbard and Franz Josef Land, Barents Sea Large Igneous Province: Geological Magazine, v. 150, p. 1127-1135.

Courtillot, V., Jaupart, C., Manighetti, I., Tapponnier, P., and Besse, J., 1999, On causal links between flood basalts and continental breakup: Earth and Planetary Science Letters, v. 166, no. 3–4, p. 177-195.

Cui, Y., and Kump, L. R., 2014, Global warming and the end-Permian extinction event: Proxy and modeling perspectives: Earth-Science Reviews.

Dallmann, W. K., Andresen, A., S.G., B., Maher, H. D., and Ohta, Y., 1993, Tertiary fold-and-thrust belt of Spitsbergen, Svalbard.: Norsk Polarinstitute Meddelelser, v. 128, p. 1-46.

Davison, R. L., Natusch, D. F. S., Wallace, J. R., and Evans, C. A., 1974, Trace elements in fly ash. Dependence of concentration on particle size: Environmental Science & Technology, v. 8, no. 13, p. 1107-1113.

Dustira, A. M., Wignall, P. B., Joachimski, M., Blomeier, D., Hartkopf-Fröder, C., and Bond, D. P. G., 2013, Gradual onset of anoxia across the Permian–Triassic Boundary in Svalbard, Norway: Palaeogeography, Palaeoclimatology, Palaeoecology, v. 374, no. 0, p. 303-313.

Ehrenberg, S. N., Pickard, N. A. H., Henriksen, L. B., Svånå, T. A., Gutteridge, P., and Macdonald, D., 2001, A Depositional and Sequence Stratigraphic Model for Cold-Water, Spiculitic Strata Based on the Kapp Starostin Formation (Permian) of Spitsbergen and Equivalent Deposits from the Barents Sea: AAPG Bulletin, v. 85, no. 12, p. 2061-2087.

Embry, A. F., 1992, Crockerland-The Northwest source area for the Sverdrup Basin, Canadian Arctic Islands, *in* Vorren, T. O., Bergsager, E., Dahl-Stamnes, Ø. A., Holter, E., Johansen, B., Lie, E., and Lund, T. B., eds., Arctic Geology and Petroleum Potential, Volume 2: Amsterdam, Elsevier, p. 205-216.

Embry, A. F., and Beauchamp, B., 2008, Sverdrup Basin, *in* Miall, A. D., ed., The Sedimentary Basins of Unites States and Canada, Elsevier, p. 451-472.

Erwin, D. H., 2006, Extinction. How life on Earth nearly ended 250 million years ago, New Jersey, Princeton University Press.

Fedo, C. M., Wayne Nesbitt, H., and Young, G. M., 1995, Unraveling the effects of potassium metasomatism in sedimentary rocks and paleosols, with implications for paleoweathering conditions and provenance: Geology, v. 23, no. 10, p. 921-924.

Fedorenko, V., Czamanske, G., Zen'ko, T., Budahn, J., and Siems, D., 2000, Field and Geochemical Studies of the Melilite-Bearing Arydzhangsky Suite, and an Overall Perspective on the Siberian Alkaline-Ultramafic Flood-Volcanic Rocks: International Geology Review, v. 42, no. 9, p. 769-804.

Frogner Kockum, P. C., Herbert, R. B., and Gislason, S. R., 2006, A diverse ecosystem response to volcanic aerosols: Chemical Geology, v. 231, no. 1–2, p. 57-66.

Furuya, K., Miyajima, Y., Chiba, T., and Kikuchi, T., 1987, Elemental characterization of particle size-density separated coal fly ash by spectrophotometry, ICP (inductively coupled plasma emission spectrometry), and scanning electron microscopy-energy dispersive x-ray analysis: Environmental Science & Technology, v. 21, no. 9, p. 898-903.

Gates, L., James, N. P., and Beauchamp, B., 2004, A glass ramp: shallow-water Permian spiculitic chert sedimentation, Sverdrup Basin, Arctic Canada: Sedimentary Geology, v. 168, p. 125-147.

Gieré, R., Carleton, L. E., and Lumpkin, G. R., 2003, Micro- and nanochemistry of fly ash from a coal-fired power plant: American Mineralogist, v. 88, no. 11-12, p. 1853-1865.

Golonka, J., and Ford, D., 2000, Pangean (Late Carboniferous-Middle Jurassic) paleoenvironment and lithofacies: Palaeogeography, Palaeoclimatology, Palaeoecology v. 161, p. 1-34.

Grasby, S. E., and Beauchamp, B., 2008, Intrabasin variability of the carbon-isotope record across the Permian-Triassic transition, Sverdrup Basin, Arctic Canada: Chemical Geology, v. 253, p. 141-150.

-, 2009, Latest Permian to Early Triassic basin-to-shelf anoxia in the Sverdrup Basin, Arctic Canada Chemical Geology, v. 264, p. 232-246.

Grasby, S. E., Beauchamp, B., Embry, A. F., and Sanei, H., 2013a, Recurrent Early Triassic ocean anoxia: Geology, v. 41, p. 175-178.

Grasby, S. E., Sanei, H., and Beauchamp, B., 2011, Catastrophic dispersion of coal fly ash into oceans during the latest Permian extinction: Nature Geoscience, v. 4, no. 2, p. 104-107.

Grasby, S. E., Sanei, H., Beauchamp, B., and Chen, Z., 2013b, Mercury deposition through the Permo–Triassic Biotic Crisis: Chemical Geology, v. 351, no. 0, p. 209-216.

Grice, K., Cao, C., Love, G. D., Böttcher, M. E., Twitchett, R. J., Grosjean, E., Summons, R. E., Turgeon, S. C., Dunning, W., and Jin, Y., 2005, Photic zone euxinia during the Permian-Triassic superanoxic event: Science, v. 307, p. 706-709.

Hall, G., and Pelchat, P., 1997, Evaluation of a Direct Solid Sampling Atomic Absorption Spectrometer for the Trace Determination of Mercury in Geological Samples: Analyst, v. 122, no. 9, p. 921-924.

Hays, L., Beatty, T., Henderson, C. M. B., Love, G. D., and Summons, R. E., 2007, Evidence for photic zone euxinia through the end-Permian mass extinction in the Panthalassic Ocean (Peace River Basin, Western Canada): Palaeoworld, v. 16, p. 39-50.

Hellman, F. J., Gee, D. G., and Witt-Nilsson, P., 2001, Late Archean basement in the Bangenhuken Complex of the Nordbreen Nappe, western Ny-Friesland, Svalbard: Polar Research, v. 20, no. 1, p. 49-59.

Henderson, C. M., and Baud, A., Correlation of the Permian-Triassic boundary in Arctic Canada and comparison with Meishan, China *in* Proceedings International Geological Congress1997, Volume 30, International Geological Congress, p. 143-152.

Hermann, E., Hochuli, P. A., Bucher, H., Vigran, J. O., Weissert, H., and Bernasconi, S. M., 2010, A close-up view of the Permian–Triassic boundary based on expanded organic carbon isotope records from Norway (Trøndelag and Finnmark Platform): Global and Planetary Change, v. 74, no. 3–4, p. 156-167.

Heydari, E., and Hassanzadeh, J., 2003, Deev Jahi Model of the Permian-Triassic boundary mass extinction: A case for gas hydrates as the main cause of biological crisis on Earth: Sedimentary Geology, v. 163, p. 147-163.

Hochuli, P. A., Hermann, E., Vigran, J. O., Bucher, H., and Weissert, H., 2010, Rapid demise and recovery of plant ecosystems across the end-Permian extinction event: Global and Planetary Change, v. 74, no. 3-4, p. 144-155.

Hoffmann, L. J., Breitbarth, E., Ardelan, M. V., Duggen, S., Olgun, N., Hassellöv, M., and Wängberg, S. Å., 2012, Influence of trace metal release from volcanic ash on growth of Thalassiosira pseudonana and Emiliania huxleyi: Marine Chemistry, v. 132–133, no. 0, p. 28-33.

Isozaki, Y., 1997, Permo-Triassic boundary superanoxia and stratified superocean: records from lost deep sea: Science, v. 276, p. 235-238.

Joachimski, M. M., Lai, X., Shen, S., Jiang, H., Luo, G., Chen, B., Chen, J., and Sun, Y., 2012, Climate warming in the latest Permian and the Permian–Triassic mass extinction: Geology, v. 40, no. 3, p. 195-198.

Johansson, Å., Larionov, A. N., Tebenkov, A. M., Ohta, Y., and Gee, D. G., 2002, Caledonian granites of western and central Nordaustlandet, northeast Svalbard: GFF, v. 124, no. 3, p. 135-148.

Jones, M. T., and Gislason, S. R., 2008, Rapid releases of metal salts and nutrients following the deposition of volcanic ash into aqueous environments: Geochimica et Cosmochimica Acta, v. 72, no. 15, p. 3661-3680.

Kaakinen, J. W., Jorden, R. M., Lawasani, M. H., and West, R. E., 1975a, Trace element behavior in coal-fired power plant: Environmental Science & Technology, v. 9, no. 9, p. 862-869.

Kaakinen, J. W., Jorden, R. M., Lawasani, M. H., and West, R. E., 1975b, Trace element behavior in coal fired power plant: Environmental Science and Technology, v. 9, no. 9, p. 862-869.

Kaiho, K., Kajiwara, Y., Nakano, T., Miura, Y., Kawahata, H., Tazaki, K., Ueshima, M., Chen, Z., and Shi, G. R., 2001, End-Permian castrophe by a bolide impact: Evidence of a gigantic release of sulfur from the mantle: Geology, v. 29, no. 9, p. 815-818.

Kaiho, K., and Koga, S., 2013, Impacts of a massive release of methane and hydrogen sulfide on oxygen and ozone during the late Permian mass extinction: Global and Planetary Change, v. 107, no. 0, p. 91-101.

Kidder, D. L., and Worsley, T. R., 2004, Causes and consequences of extreme Permo-Triassic warming to globally equable climate and relation to the Permo-Triassic extinction and recovery: Palaeogeography, Palaeoclimatology, Palaeoecology, v. 203, p. 207-237.

-, 2010, Phanerozoic Large Igneous Provinces (LIPs), HEATT (Haline Euxinic Acidic Thermal Transgression) episodes, and mass extinctions: Palaeogeography, Palaeoclimatology, Palaeoecology, v. 295, no. 1-2, p. 162-191.

Klein, D. H., Andren, A. W., Carter, J. A., Emery, J. F., Feldman, C., Fulkerson, W., Lyon, W. S., Ogle, J. C., and Talmi, Y., 1975, Pathways of thirty-seven trace elements through coal-fired power plant: Environmental Science and Technology, v. 9, p. 973-979.

Knies, J., Grasby, S. E., Beauchamp, B., and Schubert, C., 2013, Water mass denitrification during the Latest Permian Extinction in the Sverdrup Basin, Arctic Canada: Geology v. 41, p. 167-170.

Knoll, A. H., R.K. Bambach, Canfield, D. E., and Grotzinger, J. P., 1996, Comparative Earth History and Late Permian Mass Extinction: Science, v. 273, p. 452-457.

Konhauser, K. O., Pecoits, E., Lalonde, S. V., Papineau, D., Nisbet, E. G., Barley, M. E., Arndt, N. T., Zahnle, K., and Kamber, B. S., 2009, Oceanic nickel depletion and a methanogen famine before the Great Oxidation Event: Nature, v. 458, no. 7239, p. 750-753.

Korte, C., and Kozur, H. W., 2010, Carbon-isotope stratigraphy across the Permian-Triassic boundary: A review: Journal of Asian Earth Sciences, v. 39, no. 4, p. 215-235.

Korte, C., Kozur, H. W., and Partoazar, H., 2004, Neagtive carbon isotope excursion at the Permian/TRiassic boundary section at Zal, NW-Iran: Hallesches Jahrb. Geowiss, v. 18, p. 69-71.

Korte, C., Pande, P., Kalia, P., Kozur, H. W., Joachimski, M. M., and Oberhansli, H., 2010, Massive volcanism at the Permian-Triassic boundary and its impact on the isotopic composition of the ocean and atmosphere: Journal of Asian Earth Sciences, v. 37, p. 293-311.

Kump, L. R., Pavlov, A., and Arthur, M. A., 2005, Massive release of hydrogen sulfide to the surface ocean and atmosphere during intervals of oceanic anoxia: Geology, v. 33, no. 5, p. 397-400.

Lafargue, E., Espitalité, J., Marquis, F., and Pillot, D., 1998, Rock-Eval 6 applications in hydrocarbon exploration, production and soil contamination studies: Revue de L'institut Francais du Petrole v. 53, no. 4, p. 421-437.
Langmann, B., Zaksek, K., Hort, M., and Duggen, S., 2010, Volcanic ash as fertiliser for the surface ocean: Atmospheric Chemistry and Physics, v. 10, p. 3891-3899.
Lehrmann, D. J., 1999, Early Triassic calcimicrobial mounds and biostromes of Nanpanjiang basin, south China: Geology, v. 27, no. 4, p. 359-362.
Liang, H., 2002, End-Permian event of marine acidification by hydrated sulfuric acid: Mineralogical evidence from Meishan Section of South China: Chinese Science Bulletin, v. 47, p. 1393-1397.
Loope, G. R., Kump, L. R., and Arthur, M. A., 2013, Shallow water redox conditions from the Permian–Triassic boundary microbialite: The rare earth element and iodine geochemistry of carbonates from Turkey and South China: Chemical Geology, v. 351, no. 0, p. 195-208.
Ludwig, K. R., 2003, Isoplot 3.0. A Geochronological Toolkit for Microsoft Excel, Berkeley Geochronology Centre, Special Publication 4, 70 p.:
Ludwig, K. R., 2009, SQUID 2.50, A User's Manual, Berkeley, California, USA, Berkeley Geochronology Centre, 95 p.:
Maher, H. D., and Craddock, C., 1988, Decoupling as an alternate model for transpression during the initial opening of the Norwegian Greenland Sea: Polar Research, v. 6, p. 137-140.
Mangerud, G., and Konieczny, R. M., 1993, Palynology of the Permian succession of Spitsbergen, Svalbard. : Ploar Research, v. 12, p. 65-93.
Martin, R. E., 1996, Secular increase in nutrient levels throughout the Phanerozoic: implications for productivity, biomass, and diversity of the marine biosphere: Palaios, v. 11, p. 201-219.
Martinez-Tarazona, M. R., and Spears, D. A., 1996, The fate of trace elements and bulk minerals in pulverized coal combustion in a power station: Fuel Processing Technology, v. 47, no. 1, p. 79-92.
Mather, T. A., Pyle, D. M., and Oppenheimer, C., 2013, Tropospheric Volcanic Aerosol, Volcanism and the Earth's Atmosphere, American Geophysical Union, p. 189-212.
Mørk, A., Knarud, R., and Worsley, D., 1982, Depositional and diagenetic environments of the Triassic and Lower Jurassic succession of Svalbard, *in* Embry, A. F., and Balkwill, H. R., eds., Arctic geology and geophysics: proceedings of the Third International Symposium on Arctic Geology: Calgary, Canadian Society of Petroleum Geologists, p. 371-398.
Nakamura, K., Kimura, G., and Winsnes, T. S., 1987, Brachiopod zonation and age of the Permian Kapp Starostin Formation (Central Spitsbergen): Polar Research, v. 5, p. 207-219.
Nakrem, H. A., Orchard, M. J., Weitschat, W., Hounslow, M. W., Beatty, T. W., and Mørk, A., 2008, Triassic conodonts from Svalbard and their Boreal correlations: Polar Research, v. 27, p. 523-539.
Nesbitt, H. W., and Young, G. M., 1982, Early Proterozoic climates and plate motions inferred from major element chemistry of lutites: Nature, v. 299, no. 5885, p. 715-717.
Nriagu, J. O., 1989, A global assessment of natural sources of atmospheric trace metals: Nature, v. 338, no. 6210, p. 47-49.
Odasz-Albrigtsen, A. M., Tømmervik, H., and Murphy, P., 2000, Decreased photosynthetic efficiency in plant species exposed to multiple airborne pollutants along the Russian-Norwegian border: Canadian Journal of Botany, v. 78, no. 8, p. 1021-1033.

Ogden, D. E., and Sleep, N. H., 2012, Explosive eruption of coal and basalt and the end-Permian mass extinction: Proceedings of the National Academy of Sciences, v. 109, no. 1, p. 59-62.

Olsson, J., Stipp, S. L. S., Dalby, K. N., and Gislason, S. R., 2013, Rapid release of metal salts and nutrients from the 2011 Grímsvötn, Iceland volcanic ash: Geochimica et Cosmochimica Acta, v. 123, no. 0, p. 134-149.

Pacyna, J. M., and Pacyna, E. G., 2001, An assessment of global and regional emissions of trace metals to the atmosphere from anthropogenic sources worldwide: Environmental Reviews, v. 9, no. 4, p. 269-298.

Papastefanou, C., 2010, Escaping radioactivity from coal-fired power plants (CPPs) due to coal burning and the associated hazards: a review.: Journal of Environmental Radioactivity, v. 101, p. 191-200.

Pavlov, V. E., Fluteau, F., Veselovskiy, R. V., Fetisova, A. M., and Latyshev, A. V., 2011, Secular geomagnetic variations and volcanic pulses in the Permian-Triassic traps of the Norilsk and Maimecha-Kotui provinces: Izvestiya, Physics of the Solid Earth, v. 47, no. 5, p. 402-417.

Payne, J. L., Lehrmann, D., J., Follett, D., Seibel, M., Kump, L. R., Riccardi, A., Altiner, D., Sano, H., and Wei, J., 2007, Erosional truncation of uppermost Permian shallow-marine carbonates and implications for Permian-Triassic boundary events: Geological Society of America Bulletin, v. 119, no. 7/8, p. 771-784.

Payne, J. L., and van de Schootbrugge, B., 2007, Life in Triassic oceans : links between planktonic and benthic recovery and radiation, *in* Falkowski, P., and Knoll , A. H., eds., Evolution of Primary Producers in the Sea Amsterdam, Academic Press, p. 165-189.

Proemse, B. C., Grasby, S. E., Wieser, M. E., Mayer, B., and Beauchamp, B., 2013, Molybdenum isotopic evidence for oxic marine conditions during the Latest Permian extinction: Geology, v. 41, no. 9, p. 967-970.

Pyle, D. M., and Mather, T. A., 2003, The importance of volcanic emissions for the global atmospheric mercury cycle: Atmospheric Environment, v. 37, no. 36, p. 5115-5124.

Raiswell, R., and Berner, R. A., 1985, Pyrite formation in euxinic and semi-euxinic sediments: American Journal of Science, v. 285, p. 710-724.

Reichow, M. K., Pringle, M. S., Al'Mukhamedoc, A. I., Allen, M. B., Andreichev, V. L., Buslov, M. M., Davies, C. E., Fedoseev, G. S., Fitton, J. G., Inger, S., Medvedev, A. Y., Mitchell, C., Puchkov, V. N., Safonova, I. Y., Scott, R. A., and Saunders, A. D., 2009, The timing and extent of the eruption of the Siberian Traps large igneous province: Implications for the end-Permian environmental crisis: Earth and Planetary Science Letters, v. 277, p. 9-20.

Reid, C. M., James, N. P., Beauchamp, B., and Kyser, T. K., 2007, Faunal turnover and changing oceanography: Late Palaeozoic warm-to-cool water carbonates, Sverdrup Basin, Canadian Arctic Archipelago: Palaeogeography, Palaeoclimatology, Palaeoecology, v. 249, p. 128-159.

Renne, P. R., Black, M. T., Zichao, Z., Richards, M. A., and Basu, A. R., 1995, Synchrony and Causal Relations Between Permian-Triassic Boundary Crises and Siberian Flood Volcanism: Science, v. 269, no. 5229, p. 1413-1416.

Retallack, G. J., 1999, Postapocalyptic greenhouse paleoclimate revealed by earliest Triassic paleosols in the Sydney Basin, Australia: Geological Society of America Bulletin, v. 111, no. 1, p. 52-70.

Retallack, G. J., and Jahren, A. H., 2008, Methane release from igneous intrusion of coal during Late Permian extinction events: The Journal of Geology, v. 116, p. 1-20.

Retallack, G. J., and Krull, E. S., 2006, Carbon isotopic evidence for terminal-Permian methane outbursts and their role in extinctions of animals, plants coral reefs, and peat swamps, *in* Greb, S. F., and DiMichele, W. A., eds., Wetlands through time: Geological Society of America Special Paper 399, p. 249-268.

Richoz, S., Krystyn, L., Baud, A., Brandner, R., Horacek, M., and Mohtat-Aghai, P., 2010, Permian–Triassic boundary interval in the Middle East (Iran and N. Oman): Progressive environmental change from detailed carbonate carbon isotope marine curve and sedimentary evolution: Journal of Asian Earth Sciences, v. 39, no. 4, p. 236-253.

Romano, C., Goudemand, N., Vennemann, T. W., Ware, D., Schneebeli-Hermann, E., Hochuli, P. A., Bruhwiler, T., Brinkmann, W., and Bucher, H., 2013, Climatic and biotic upheavals following the end-Permian mass extinction: Nature Geosci, v. 6, no. 1, p. 57-60.

Rothman, D. H., Fournier, G. P., French, K. L., Alm, E. J., Boyle, E. A., Cao, C., and Summons, R. E., 2014, Methanogenic burst in the end-Permian carbon cycle: Proceedings of the National Academy of Sciences, v. 111, no. 15, p. 5462-5467.

Ruggieri, F., Fernández-Turiel, J.-L., Saavedra, J., Gimeno, D., Polanco, E., and Naranjo, J. A., 2011, Environmental geochemistry of recent volcanic ashes from the Southern Andes: Environmental Chemistry, v. 8, no. 3, p. 236-247.

Sanei, H., Grasby, S. E., and Beauchamp, B., 2012, Latest Permian mercury anomalies: Geology, v. 40, no. 1, p. 63-66.

Saunders, A. D., and Reichow, M. K., 2009, The Siberian Traps and the End-Permian mass extinction: a critical review: Chinese Science Bulletin, v. 54, p. 20-37.

Schoepfer, S. D., Henderson, C. M., Garrison, G. H., Foriel, J., Ward, P. D., Selby, D., Hower, J. C., Algeo, T. J., and Shen, Y., 2013, Termination of a continent-margin upwelling system at the Permian–Triassic boundary (Opal Creek, Alberta, Canada): Global and Planetary Change, v. 105, no. 0, p. 21-35.

Scotese, C. R., 2004, A continental drift flipbook: Journal of Geology, v. 112, p. 729-741.

Scott, C., and Lyons, T. W., 2012, Contrasting molybdenum cycling and isotopic properties in euxinic versus non-euxinic sediments and sedimentary rocks: Refining the paleoproxies: Chemical Geology, v. 324-325, p. 19-27.

Sephton, M. A., Looy, C. V., Brinkhuis, H., Wignall, P. B., de Leeuw, J. W., and Visscher, H., 2005, Catastrophic soil erosion during the end-Permian biotic crisis Geology, v. 33, no. 12, p. 941-944.

Sheldon, N. D., 2006, Abrupt chemical weathering increase across the Permian-Triassic boundary: Palaeogeography, Palaeoclimatology, Palaeoecology, v. 231, p. 315-321.

Shen, S.-z., Crowley, J. L., Wang, Y., Bowring, S. A., Erwin, D. H., Sadler, P. M., Cao, C.-q., Rothman, D. H., Henderson, C. M., Ramezani, J., Zhang, H., Shen, Y., Wang, X.-d., Wang, W., Mu, L., Li, W.-z., Tang, Y.-g., Liu, X.-l., Liu, L.-j., Zeng, Y., Jiang, Y.-f., and Jin, Y.-g., 2011, Calibrating the End-Permian Mass Extinction: Science.

Sial, A. N., Lacerda, L. D., Ferreira, V. P., Frei, R., Marquillas, R. A., Barbosa, J. A., Gaucher, C., Windmöller, C. C., and Pereira, N. S., 2013, Mercury as a proxy for volcanic activity during extreme environmental turnover: The Cretaceous–Paleogene transition: Palaeogeography, Palaeoclimatology, Palaeoecology, v. 387, no. 0, p. 153-164.

Silva, M. V. N., Sial, A. N., Barbosa, J. A., Ferreira, V. P., Neumann, V. H., and De Lacerda, L. D., 2013, Carbon isotopes, rare-earth elements and mercury geochemistry across the K–T transition of the Paraíba Basin, northeastern Brazil: Geological Society, London, Special Publications, v. 382.

Smith, R. D., Campbell, J. A., and Nielson, K. K., 1979, Concentration dependence upon particle size of volatilized elements in fly ash: Environmental Science & Technology, v. 13, no. 5, p. 553-558.

Song, H., Wignall, P. B., Chu, D., Tong, J., Sun, Y., Song, H., He, W., and Tian, L., 2014, Anoxia/high temperature double whammy during the Permian-Triassic marine crisis and its aftermath: Sci. Rep., v. 4.

Stacey, J. S., and Kramers, J. D., 1975, Approximation of terrestrial lead isotope evolution by a two-stage model: Earth and Planetary Science Letters v. 26, p. 207-221.

Stemmerik, L., and Worsley, D., 1995, Permian History of the Barents Shelf Area, *in* Scholle, P., Peryt, T., and Ulmer-Scholle, D., eds., The Permian of Northern Pangea, Springer Berlin Heidelberg, p. 81-97.

Stemmerik, L., and Worsley, D., 2005, 30 years on - Arctic Upper Palaeozoic stratigraphy, depositional evolution and hydrocarbon prospectivity: Norsk Geologisk Tidsskrift v. 85, p. 151-168.

Stern, R. A., 2001, Radiogenic age and isotopic studies: Report 14. , Volume Current Research 2001-F1, Geological Survey of Canada, p. 11pp.

Stern, R. A., S., B., S.L., K., Hickman, A. H., and F., C., 2009, Measurement of SIMS instrumental mass fractionation of Pb-isotopes during zircon dating: Geostandards and Geoanalytical Research, v. 33, p. 145-168.

Sun, Y., Joachimski, M. M., Wignall, P. B., Yan, C., Chen, Y., Jiang, H., Wang, L., and Lai, X., 2012, Lethally Hot Temperatures During the Early Triassic Greenhouse: Science, v. 338, no. 6105, p. 366-370.

Svensen, H., Planke, S., Polozov, A. G., Schmidbauer, N., Corfu, F., Podladchikov, Y. Y., and Jamtveit, B., 2009, Siberian gas venting and the end-Permian environmental crisis: Earth and Planetary Science Letters, v. 277, p. 490-500.

Sydeman, W. J., García-Reyes, M., Schoeman, D. S., Rykaczewski, R. R., Thompson, S. A., Black, B. A., and Bograd, S. J., 2014, Climate change and wind intensification in coastal upwelling ecosystems: Science, v. 345, no. 6192, p. 77-80.

Symonds, R. B., Rose, W. I., Reed, M. H., Lichte, F. E., and Finnegan, D. L., 1987, Volatilization, transport and sublimation of metallic and non-metallic elements in high temperature gases at Merapi Volcano, Indonesia: Geochimica et Cosmochimica Acta, v. 51, no. 8, p. 2083-2101.

Taylor, S. R., and McLennan, S. M., 1985, The Continental Crust: its Composition and Evolution, Oxford, Blackwell, 312 p.:

Tozer, E. T., and Parker, J. R., 1968, Notes on the Triassic biostratigraphyof Svalbard: Geological Magazine v. 105, p. 526-542.

Tribovillard, N., Algeo, T. J., Lyons, T., and Riboulleau, A., 2006, Trace metals as paleoredox and paleoproductivity proxies: An update: Chemical Geology, v. 232, no. 1–2, p. 12-32.

Twitchett, R. J., Looy, C. V., Morante, R., Visscher, H., and Wignall, P. B., 2001, Rapid and synchrous collapse of marine and terrestrial ecosystems during the end-Permian biotic crisis: Geology, v. 29, no. 4, p. 351-354.

Vie le Sage, R., 1983, Chemistry of the volcanic aerosol, Elsevier, p. 445-474.

Wang, K., Geldsetzer, H. H. J., and Krouse, H. R., 1994, Permian-Triassic extinction: Organic $\delta^{13}C$ evidence from British Columbia, Canada: Geology, v. 22, p. 580-584.

White, R. V., and Saunders, A. D., 2005, Volcanism, impact and mass extinctions: incredible or credible coincidences?: Lithos, v. 79, no. 3–4, p. 299-316.

Wignall, P., and Newton, R., 2003, Contrasting deep-water records from the Upper Permian and Lower Triassic of South Tibet and British Columbia; evidence for a diachronous mass extinction: Palaios, v. 18, p. 153-167.

Wignall, P. B., 2001, Large igneous provinces and mass extinctions: Earth-Science Reviews, v. 53, no. 1-2, p. 1-33.

Wignall, P. B., and Hallam, A., 1992, Anoxia as a cause of the Permian/Triassic mass extinction; facies evidence from northern Italy and the Western United States Palaeogeography, Palaeoclimatology, Palaeoecology, v. 93, no. 1-2, p. 21-46.

Wignall, P. B., Morante, R., and Newton, R., 1998, The Permo-Triassic transition in Spitsbergen: $\delta^{13}C_{org}$ chemostratigraphy, Fe and S geochemistry, facies, fauna and trace fossils: Geologic Magazine, v. 135, p. 47-62.

Wignall, P. B., and Twitchett, R. J., 1996, Oceanic anoxia and the end Permian mass extinction Science, v. 272, no. 5265, p. 1155-1158.

Williams, I. S., 1998, U-Th-Pb Geochronology by Ion Microprobe, *in* McKibben, M. A., Shanks, W. C., and Ridely, W. I., eds., Applications of Microanalytical Techniques to Understanding Mineralizing Processes,, p. 1-35.

Xie, S., Pancost, R. D., Huang, J., Wignall, P. B., Yu, J., Tang, X., Chen, L., Huang, X., and Lai, X., 2007, Changes in the global carbon cycle occured as two episodes during the Permina-Triassic crisis: Geology, v. 35, no. 12, p. 1083-1086.

Xie, S., Pancost, R. D., Wang, Y., Yang, H., Wignall, P. B., Luo, G., Jia, C., and Chen, L., 2010, Cyanobacterial blooms tied to volcanism during the 5 m.y. Permo-Triassic biotic crisis: Geology, v. 38, no. 5, p. 447-450.

Xie, S., Pancost, R. D., Yin, H., Wang, H., and Evershed, R. P., 2005, Two episodes of microbial change coupled with Permo/Triassic faunal mass extinction: Nature, v. 434, p. 494-497.

Yin, H., Zhang, K., Tong, J., Yang, Z., and Wu, S., 2001, The global stratotype section and point (GSSP) of the Permian-Triassic boundary: Episodes, v. 24, p. 102-117.

Table captions

Table 1: SHRIMP U-Pb zircon data for the ash layer. Ages are quoted as $^{206}Pb/^{238}U$ dates for Paleozoic zircons and as $^{207}Pb/^{206}Pb$ dates for Archean zircons.

Table 2: Geochemical data from the Festningen section. TC= total carbon, TOC = total organic carbon, TIC = total inorganic carbon, CIA = chemical index of alteration, n.d. = not determined.

Table 3: Calculated increase in metal loading rates due to the Siberian Trap eruptions, based on metal/S ratio of Nriagu (1989) (mid point of the range given was used) and total S flux of Siberian Trap Volcanism (Beerling et al., 2007). Two loading rates are calculated for a

constant eruption rated over 500 ky, or a sporatic eruption over a net 40 ky time period. Natural modern flux from Pacyna and Pacyna (2001).

Figure Captions

Figure 1 Location maps of field area, showing A) global Late Permian reconstruction base map after R. Scotese, B) the location of the Festningen section on Spitsbergen, and C) the paleo locations of important sedimentary records on the NW margin of Pangea at the time of the LPE event (Embry, 1992).

Figure 2 Field photographs of the Festningen section, showing: A) the top resistant bedding plane of the Kapp Starostin Formation and overlying sediments of the Vardebukta Formation, B) basal shales of the Vardebukta Formation, location shown in Fig. 2a, and C) close up of finely laminated shales that mark the loss of burrowers in the section, location in Fig. 2b.

Figure 3 Results of age dating, showing A) Cathodoluminescence images and ages of selected zircons of the ash layer, and B) concordia plot of SHRIMP data for zircon grains from the ash layer.

Figure 4 Plots of geochemical data from Festningen, including: A) $\delta^{13}C$ of organic carbon, B) percent total organic carbon (TOC), C) percent total inorganic carbon (TIC), D) nitrogen isotope values, E) chemical index of alteration (Sydeman et al.).

Figure 5 Plots of redox sensitive indicators for Festningen, including: A) percent Fe pyrite (Fepy), B) Molybdenum (Mo), C) uranium (U), and D) vanadium (V). Solid circles show absolute concentrations whereas dashed lined represent normalised values.

Figure 6 Geochemical plot of: A) percent total sulfur (TS) versus total organic carbon (TOC) showing the significant shift to more anoxic state after the first ash bed (white circles), B) inverse relationship between carbon isotope values and redox proxies across the extinction horizon.

Figure 7 Plot of trace metals along with A) carbon isotope values, and B) Mo for reference. Trends in metals across the extinction horizon include: C) Cu, D) Pb, E) As, F) Co, G) Ni, E) trends of Hg normalised to total organic carbon (TOC). Average shale values are shown as vertical dashed lines derived from Taylor and McLennan (1985) for Pb, Co, Ni, and Wedepohl (1991) for Cu, and As. Colour bars represent interpreted major impacts on life across the extinction event, including initial marine water acidity, development of toxicity, then finally anoxia.

Figure 8 Comparative plot of key sections from NW Pangea, Festningen (this study) and West Blind Fiord, Sverdrup Basin (Proemse et al., 2013). Note that the sections were vertically scaled to align the Latest Permian Extinction (LPE) event and the assumed Permian-Triassic Boundary (PTB) in both sections. Position of the PTB based on Algeo et al. (2012) and Wignall et al. (1998). The scale difference reflects higher rates of subsidence at West Blind Fiord than at Festningen. Note that the lower ash layer aligns perfectly in both sections.


A)
Spitsbergen
C)
Panthalassa
Tethys
Siberian Traps
Pangea
Neotethys
B)
0 km 100
80°
79°
78°
77°
SPITSBERGEN
Isfjorden
Nordenskiöld Land
Festningen
N
15°
21°
27°
C)
ALASKA
RUSSIA
CHUKCHI
CROCKER LAND
SVERDRUP BASIN
SVALBARD
BARENTS SEA
CANADA
GREENLAND

Figure 1

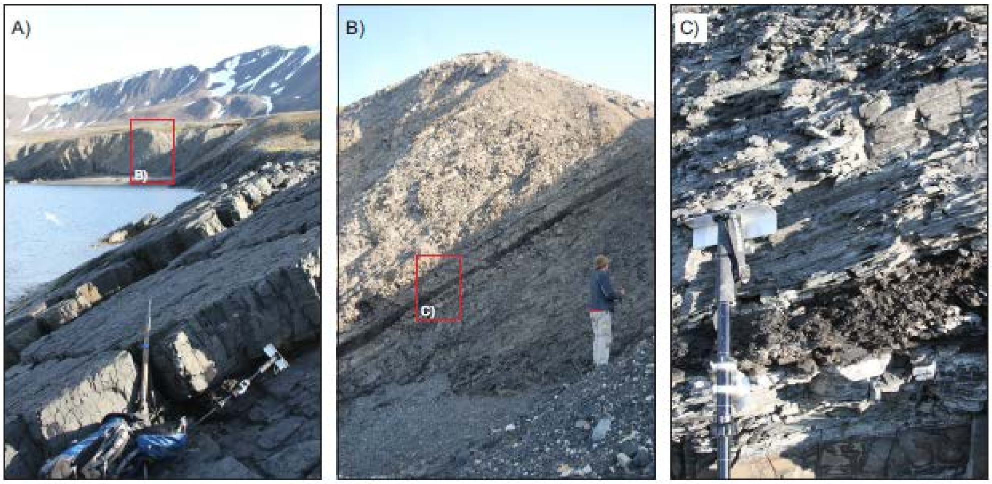

Figure 2

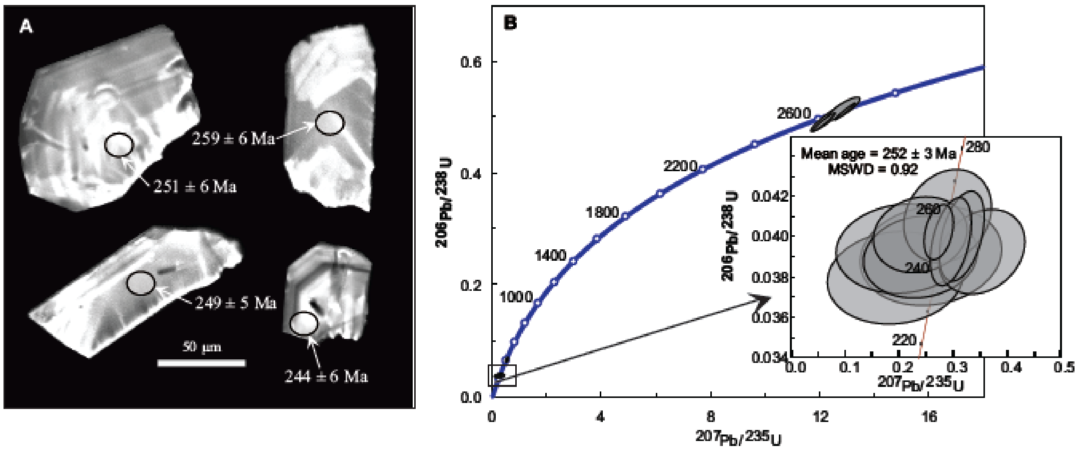
A
259 ± 6 Ma
251 ± 6 Ma
249 ± 5 Ma
244 ± 6 Ma
50 µm
B
Mean age = 252 ± 3 Ma
MSWD = 0.92
206Pb/238U
207Pb/235U

Figure 3

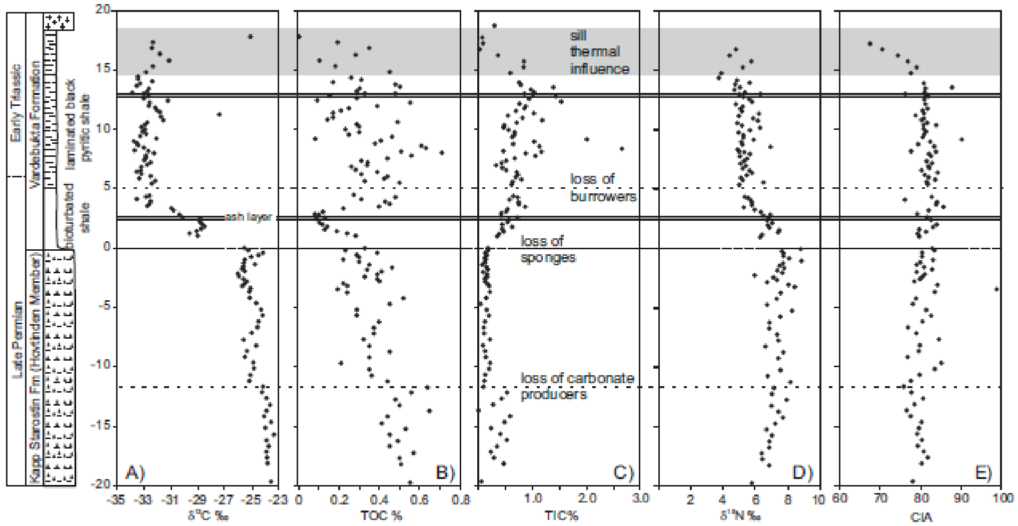
Early Triassic
Late Permian
Vardebukta Formation
Kapp Starostin Fm (Hovtinden Member)
laminated black pyritic shale
bioturbated shale
ash layer
sill thermal influence
loss of burrowers
loss of sponges
loss of carbonate producers
A)
B)
C)
D)
E)
TOC %
TIC%
CIA

Figure 4

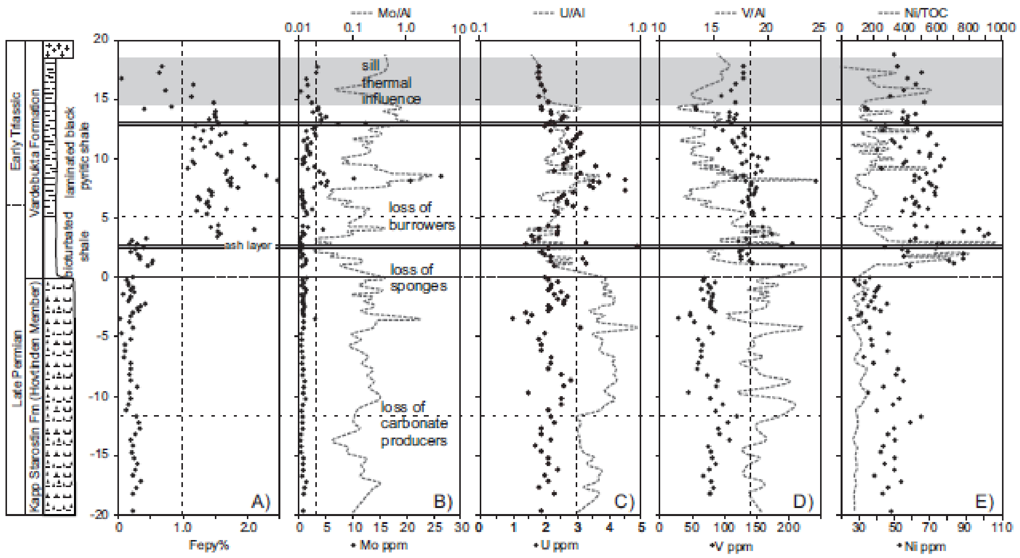

Mo/Al
U/Al
V/Al
Ni/TOC
Early Triassic
Vardebukta Formation
laminated black pyritic shale
bioturbated shale
Late Permian
Kapp Starostin Fm (Hovtinden Member)
sill thermal influence
ash layer
loss of burrowers
loss of sponges
loss of carbonate producers
A)
B)
C)
D)
E)
Fepy%
Mo ppm
U ppm
V ppm
Ni ppm

Figure 5

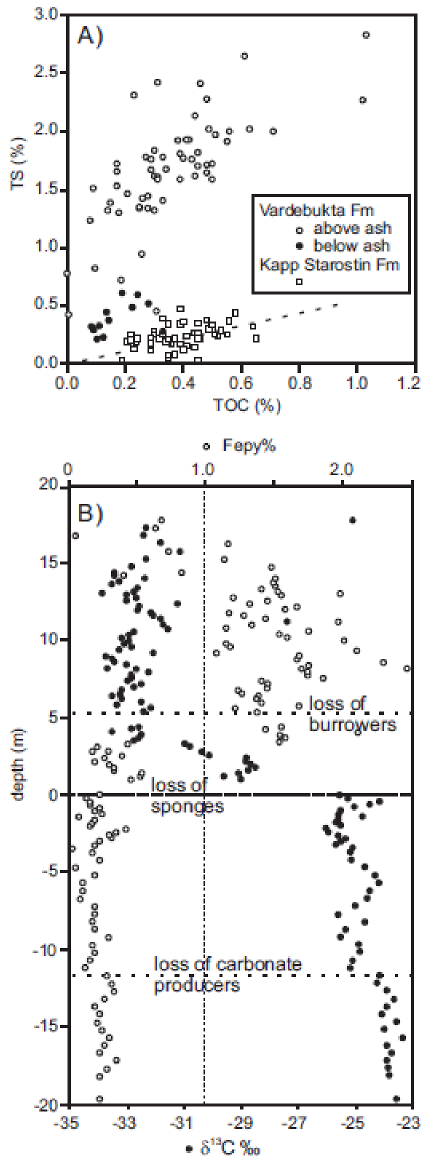
A)
TS (%)
TOC (%)
Vardebukta Fm
above ash
below ash
Kapp Starostin Fm
B)
Fepy%
depth (m)
loss of burrowers
loss of sponges
loss of carbonate producers
δ13C ‰

Figure 6

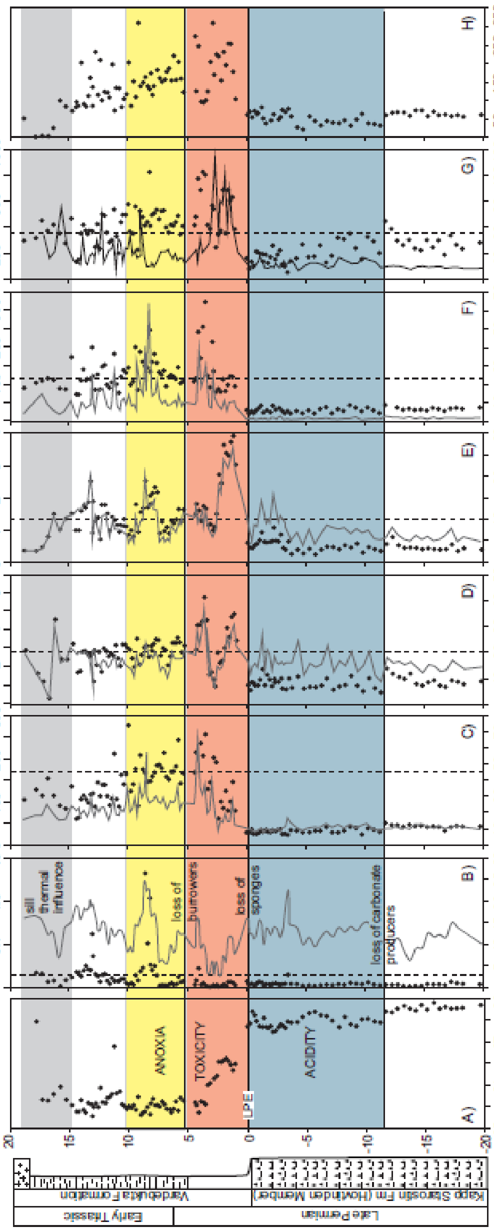
A)
B)
C)
D)
E)
F)
G)
H)
ANOXIA
TOXICITY
ACIDITY
LPE
still thermal influence
loss of burrowers
loss of sponges
loss of carbonate producers
Mo/Al
Cu/Al
Pb/Al
As/Al
Co/Al
Ni/TOC
Hg/TOC
Mo ppm
Cu ppm
Pb ppm
As ppm
Co ppm
Ni ppm
Early Triassic
Late Permian
Vardebukta Formation
Kapp Starostin Fm (Hovtinden Member)

Figure 7

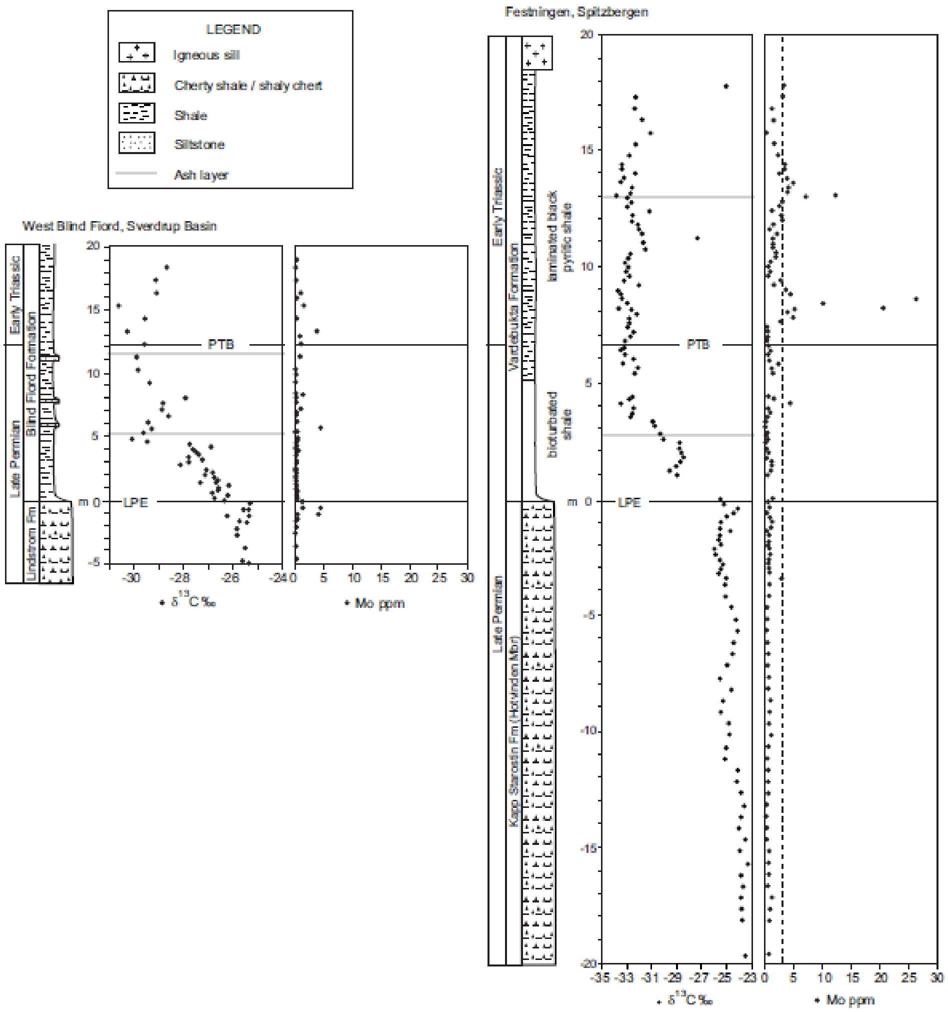
LEGEND
Igneous sill
Cherty shale / shaly chert
Shale
Siltstone
Ash layer
West Blind Fiord, Sverdrup Basin
Festningen, Spitzbergen
Early Triassic
Late Permian
Blind Fiord Formation
Lindstrom Fm
Vardebukta Formation
Kapp Starostin Fm (Hovtinden Mbr)
laminated black pyritic shale
bioturbated shale
PTB
LPE
m
δ13C ‰
Mo ppm

Figure 8